Dual Targeting of Histone Deacetylases and MYC as Potential Treatment Strategy for H3-K27M Pediatric Gliomas

Danielle Algranati[1+], Roni Oren[2+], Bareket Dassa[3], Liat Fellus-Alyagor[2], Alexander Plotnikov[4], Haim Barr[4], Alon Harmelin[2], Nir London[5], Guy Ron[6], Noa Furth[1*] and Efrat Shema[1*]

[1]Department of Immunology and Regenerative Biology, Weizmann Institute of Science, Rehovot 76100, Israel.

[2]Department of Veterinary Resources, Weizmann Institute of Science, Rehovot 76100, Israel.

[3]Bioinformatics Unit, Department of Life Sciences Core Facilities, Faculty of Biochemistry, Weizmann Institute of Science, Rehovot 76100, Israel

[4]Wohl Institute for Drug Discovery of the Nancy and Stephen Grand Israel National Center for Personalized Medicine, Weizmann Institute of Science, Rehovot 76100, Israel

[5]Department of Chemical and Structural Biology, Weizmann Institute of Science, Rehovot 76100, Israel.

[6]Racah Institute of Physics, Hebrew University, Jerusalem 91904, Israel.

* Corresponding authors:

Efrat.shema@weizmann.ac.il

Noa.furth@weizmann.ac.il

[+] Equal contribution

Abstract

Diffuse midline gliomas (DMG) are aggressive and fatal pediatric tumors of the central nervous system that are highly resistant to treatments. Lysine to methionine substitution of residue 27 on histone H3 (H3-K27M) is a driver mutation in DMGs, reshaping the epigenetic landscape of these cells to promote tumorigenesis. H3-K27M gliomas are characterized by deregulation of histone acetylation and methylation pathways, as well as the oncogenic MYC pathway. In search of effective treatment, we examined the therapeutic potential of dual targeting of histone deacetylases (HDACs) and MYC in these tumors. Treatment of H3-K27M patient-derived cells with Sulfopin, an inhibitor shown to block MYC-driven tumors *in-vivo*, in combination with the HDAC inhibitor Vorinostat, resulted in substantial decrease in cell viability. Moreover, transcriptome and epigenome profiling revealed synergistic effect of this drug combination in downregulation of prominent oncogenic pathways such as mTOR. Finally, *in-vivo* studies of patient-derived orthotopic xenograft models showed significant tumor growth reduction in mice treated with the drug combination. These results highlight the combined treatment with PIN1 and HDAC inhibitors as a promising therapeutic approach for these aggressive tumors.

Introduction

Diffuse midline gliomas (DMGs) are fatal tumors of the central nervous system that occur primarily in children[1,2]. Years of clinical trials have revealed that conventional chemotherapy is ineffective, and with no option for complete resection, DMG is now the leading cause of brain tumor-related death in children[3,4]. Sequencing studies showed that up to 80% of the diagnosed children exhibit a lysine 27 to methionine (H3-K27M) mutation in one of the genes encoding histone H3.3 and H3.1 (clinically classified as DMG, H3 K27M–mutant). Numerous subsequent studies revealed pronounced alterations in the epigenetic landscape driven by this histone mutation[5–8]. Among these global epigenetic alterations are a drastic loss of H3 lysine 27 tri-methylation (H3K27me3), concomitant with an increase in H3 lysine 27 acetylation (H3K27ac). These epigenetic alterations were shown to affect transcriptional programs and support tumorigenesis [9–14].

Detailed characterization of the modes of chromatin deregulation in these tumors pointed toward targeting epigenetic pathways as a promising therapeutic approach[15]. Specifically, pervasive H3K27 acetylation patterns observed in H3-K27M DMGs, along with enrichment of H3K27ac specifically on mutant nucleosomes[11–13,16], underscored the histone acetylation pathway as a potential drug target for this cancer. Indeed, pan-histone deacetylase inhibitors (HDACi), such as Vorinostat and Panobinostat, were found to inhibit growth and to restore gene expression alterations observed in H3-K27M malignant gliomas[17–19]. However, recent studies demonstrated that H3-K27M cells develop resistance to HDACi treatment[17,19], stressing the importance of identifying novel drug combinations to induce synergistic inhibition of oncogenic pathways.

The MYC oncogenic pathway is frequently deregulated in diverse cancers, and thus stands as a prominent therapeutic target[20]. High-level gene amplification of *MYC* is recurrently observed in pediatric high-grade gliomas[21,22]. H3-K27M gliomas show high expression of *MYC* and MYC target genes, due to both epigenetic alterations and structural variants, resulting in a viability dependency on MYC signaling[12,23,24]. Unfortunately, there are currently no clinical inhibitors to directly target the MYC protein[25]. However, Dubiella et al. have recently developed a unique inhibitor targeting Peptidyl-prolyl isomerase NIMA-interacting-1 (PIN1), an upstream regulator of MYC activation[26]. PIN1 itself is frequently upregulated in many types of cancers, resulting in sustained proliferative signaling and tumor growth[27,28]. The PIN1 inhibitor, Sulfopin, was shown to downregulate MYC target genes *in-vitro* and to block MYC-driven tumors in murine models of neuroblastoma[26].

To address the increasing need for an effective combination therapy for H3-K27M DMGs, we tested whether dual targeting of histone acetylation and MYC activation, using Vorinostat and

Sulfopin, would yield beneficial outcome. We show that the combined treatment substantially reduces viability of patient-derived glioma cells, in concordance with inhibition of prominent oncogenic pathways, including the mTOR pathway. Treatment of H3-K27M DMG xenograft mice models with this drug combination led to reduced tumor growth and confirmed downregulation of mTOR *in-vivo*. Together, these results suggest the combination of PIN1 and HDAC inhibitors as a promising therapeutic strategy for H3-K27M gliomas.

Results

Sulfopin inhibits MYC targets and reduces viability of H3-K27M glioma cells

In light of the important role of MYC in H3-K27M DMGs, we set to explore whether the PIN1 inhibitor, Sulfopin, may affect MYC signaling in these cells and thus confer therapeutic potential. Sulfopin dependent inhibition of PIN1 was shown to downregulate the expression of MYC target genes in several cancer cell lines[26]. Indeed, RNA sequencing analysis of patient-derived glioma cells (SU-DIPG13) treated with Sulfopin revealed strong enrichment of MYC targets among the downregulated genes (Fig. 1A). The genes downregulated by Sulfopin were also enriched for MYC-bound genes identified in several non-glioma cell lines, supporting a role for PIN1 in activation of the MYC pathway also in these glioma cells (Fig. S1A-B). Of note, Sulfopin was developed as a covalent inhibitor of PIN1, and did not lead to PIN1 degradation, as previously shown (Fig. S1C) [26]. We further validated the decreased expression of prominent MYC targets[27,29,30] upon Sulfopin treatment by RT-qPCR analysis (Fig. 1B). Interestingly, Cut&Run analysis[31] revealed an increase in H3K27me3 levels, indicative of repressed chromatin[32], around the transcriptional start sites (TSS) of MYC target genes, confirming epigenetic silencing of these genes upon PIN1 inhibition (Fig. 1C, S1D). Of note, global H3K27me3 distribution on all TSS and gene-body regions was not affected by Sulfopin treatment, supporting a specific increase in H3K27me3 on the TSS of MYC target genes (Fig. S1E-F). Furthermore, Sulfopin-unique H3K27me3 peaks (i.e., peaks that were found only in the Sulfopin-treated cells, and not in DMSO-treated cells) were enriched for MYC target genes (Fig. 1D).

We next explored the effect of Sulfopin on the viability of eight patient derived DMG cultures, harboring either the H3.3-K27M or H3.1-K27M mutation. In line with downregulation of MYC signaling, Sulfopin treatment led to a mild reduction in cell viability, conserved across the different cultures (Fig. 1E). To examine whether H3-K27M mutation renders DMG cells more sensitive to Sulfopin treatment, we took advantage of two sets of isogenic patient-derived DMG cell-lines (SU-DIPG13, BT245) in which the *H3F3A*-K27M mutant allele has been knocked-out (KO). In both lines, the reduction in cell viability was partially rescued in the KO cells (Fig. 1F), suggesting higher sensitivity of H3-K27M mutant cells to MYC inhibition by Sulfopin.

86 These results are in line with previous reports showing H3-K27M-dependent activation of the
87 MYC/RAS axis in mouse and human cells[12,23,24]. Of note, DMG cells showed greater sensitivity
88 to the inhibitor compared to human astrocytic-like cells (Fig. S1G).

89 To further explore the status of MYC and PIN1 as indicators of response to Sulfopin inhibition,
90 we analyzed published transcriptomic dataset of DMG tumors[35]. Interestingly, while DMG
91 samples showed significantly higher expression of MYC and its target genes compared to
92 normal samples, PIN1 expression was lower in the cancer compared to matched normal tissue
93 (Fig. S1H-J). Furthermore, H3-K27M mutant tumors showed higher expression of MYC,
94 compared to H3 WT tumors, while PIN1 levels were reduced across samples[22] (Fig. S1K-L).
95 These results suggest that MYC expression levels, and not PIN1, may determine the sensitivity
96 of H3-K27M cells to Sulfopin treatment. To examine this notion, we measured the expression
97 levels of MYC, as well as the doubling time of the different DMG cultures. The response to
98 Sulfopin treatment (as reflected by IC50 measurements) correlated with the cells' doubling time
99 (Fig. S1M). Cells that divide faster were more sensitive to Sulfopin treatment, in line with PIN1
100 role in regulating cell cycle progression, and specifically G2/M transition[36,37]. As expected, the
101 doubling time negatively correlated with MYC expression, suggesting that MYC levels may
102 predict the response to Sulfopin (Fig S1N). Indeed, MYC levels negatively correlated with the
103 IC50 of Sulfopin, thus, cells relaying on high MYC activity showed higher sensitivity to
104 Sulfopin (Fig S1O).

105 H3K27me3 levels were shown to be drastically deregulated in DMG cells expressing H3-
106 K27M, with global loss of this modification across the genome, and retention of residual
107 H3K27me3 at CpG islands (CGIs). These residual H3K27me3 levels were shown to be
108 necessary to silence tumor suppressor genes and maintain cell proliferation in DMG cells[33,34] .
109 Interestingly, Sulfopin treatment resulted in reduction of H3K27me3 signal over CGIs, perhaps
110 contributing to Sulfopin-dependent growth inhibition in these cells (Fig. S1P). Taken together,
111 our results indicate that PIN1 inhibition by Sulfopin downregulated MYC target genes, reduced
112 H3K27me3 levels at CGIs, and led to reduce viability of DMG cells in a H3-K27M-dependant
113 manner.

114 **Combination of Sulfopin and Vorinostat elicits robust inhibition of oncogenic pathways**
115 **and an additive effect on cell viability**

116 Inspired by the positive outcome of combinatorial drug therapy in H3-K27M DMG models[17,38],
117 we aimed to explore whether combining Sulfopin treatment with an epigenetic drug will further
118 reduce cell viability. H3-K27M gliomas are characterized by deregulation of epigenetic
119 pathways affecting post-translational modifications of lysine 27 (methylation and acetylation)
120 and lysine 4 (methylation) on histone H3[9–12,16,39]. Thus, we explored the effects of combining

121 Sulfopin with four epigenetic inhibitors targeting critical components associated with these
122 modifications: (1) EPZ-6438, an inhibitor of EZH2, the catalytic subunit of the PRC2 complex
123 that deposits H3K27me3[40]. H3-K27M cells were reported to be sensitive to EZH2 inhibition as
124 they rely on the residual H3K27me3 levels to suppress key tumor-suppressor genes[13,33,41,42]; (2)
125 GSK-J4, an inhibitor of the H3K27me3 demethylase JMJD3[43], shown to rescue H3K27me3
126 levels in H3-K27M gliomas[17,44]; (3) MM-102, an inhibitor of the H3K4me3 methyltransferase
127 MLL1[40], shown to reduce viability of H3-K27M-mutant cells[16]; and (4) Vorinostat, an HDAC
128 inhibitor that was shown to have clinical benefit in H3-K27M gliomas[17–19]. We found that the
129 combination of Sulfopin and Vorinostat (HDACi) had the strongest effect, reducing viability
130 by 80% (Fig. S2A).

131 Next, we adjusted treatment protocols to account for the optimal treatment period for each drug,
132 and examined the effect of this drug combination on the viability of eight patient-derived DMG
133 cultures, across different dosages (Fig. 2A-B and S2B-D). For each pair of concentrations, we
134 calculated a BLISS index; an additive effect of the two drugs was determined as BLISS index
135 ~1[45,46] (Fig. 2C, S2E). While the combined treatment was effective in all the cultures, cells
136 harboring H3.3-K27M showed higher sensitivity (Fig. 2D, S2F). Moreover, while an additive
137 effect of Sulfopin and Vorinostat was detected in all the H3.3-K27M DMG cultures in most of
138 the drug doses, for the H3.1-K27M cultures we measured an additive effect only in higher
139 dosages of Vorinostat (Fig. 2C-E and S2E-F). In line with the difference in sensitivity, H3.1-
140 and H3.3-K27M cells differed substantially in MYC expression levels, with H3.1-K27M cells
141 expressing significantly lower levels of MYC (Fig. S2G). Indeed, BLISS indexes negatively
142 correlated with MYC expression levels (Fig. 2F), indicating that H3.3-K27M cells, which
143 express higher levels of MYC, are more sensitive to the combination of Sulfopin and
144 Vorinostat. Importantly, this highlights MYC, and MYC target genes, as potential biomarkers
145 of response for the combined treatment. For example, the expression levels of the two MYC
146 targets, NOC4L and PSMD3, negatively correlated with the BLISS indexes and significantly
147 differed between H3.1- and H3.3-K27M cells (Fig. 2F and S2H). Furthermore, these and
148 additional MYC targets were downregulated following the combined treatment in the H3.3-
149 K27M culture, SU-DIPG13 (Fig. S2I). Overall, our data demonstrates that combining Sulfopin
150 treatment with Vorinostat results in an additive effect on the viability of DMG cultures, with
151 H3.3-K27M cells showing higher sensitivity. This is in line with previous studies highlighting
152 clinical and molecular distinction between H3.1- and H3.3-K27M mutant tumors, which is
153 thought to dictate their targetable vulnerabilities[5,47,48].

154 To gain more insights on the molecular mechanisms underlying this effect on viability, we
155 profiled the transcriptome of SU-DIPG13 cells (H3.3-K27M) treated with each of the drugs
156 alone and the combined treatment (Fig. S2J). A total of 494 genes were significantly

differentially expressed (DE) in cells treated with the drug combination, compared to only 145 and 167 in cells treated solely with Sulfopin or Vorinostat, respectively (Fig. S2K-L). Hierarchical clustering of all 620 DE genes confirmed strong additive effect of the combined treatment on gene expression, primarily demonstrated by clusters 1 and 4 (Fig. 2G). Cluster 1, consisting of approximately half of the DE genes, was strongly downregulated by the combined treatment, compared to single-agent treated cells. This cluster included genes that play crucial roles in glioma progression such as *MTOR*, *ATF3*, *CREB3 and TGFA*[49–52] (Fig. S2M). Moreover, the mTORC1 signaling pathway was highly enriched within the genes comprising cluster 1 (Fig. S2N). Importantly, GSEA analysis revealed that this pathway was significantly enriched in downregulated genes following the combined treatment (Fig. 2H and S2O). Of note, additional epigenetic and oncogenic pathways such as BMI1, cAMP and IL-6/JAK/STAT3 were significantly downregulated in cells treated with the drug combination[53–55] (Fig. 2I and S2O). Reduction in mTOR signaling (mTOR, phospho-mTOR and phospho-S6[56]) and ATF3 was further validated by western blot and RT-qPCR analysis (Fig. 2J, S2P). Importantly, we also confirmed that the combined treatment with Sulfopin and Vorinostat led to induction of p21 (CDKN1A), a prominent tumor suppressor promoting cell cycle arrest and regulated by mTOR signaling[57–59] (Fig. 2H, J). Finally, exploring mTOR expression in all the tested DMG cultures, revealed a strong negative correlation with the BLISS indexes of the combined treatment (Fig. S2Q), suggesting mTOR as a potential biomarker of response for the combined treatment of Sulfopin and Vorinostat. Overall, our data revealed that the combined inhibition of HDACs and MYC results in robust downregulation of prominent oncogenic pathways.

Sulfopin attenuates HDACi-mediated accumulation of H3K27ac on genomic regions associated with oncogenic pathways

We next examined epigenetic features that may underly the inhibition of oncogenic pathways by the combined treatment. Inhibition of histone deacetylases is expected to increase and alter genome-wide histone acetylation patterns, including the H3K27ac mark associated with active promoters and enhancers[60]. Indeed, global quantification by single-molecule measurements of H3K27-acetylated nucleosomes, as well as western blot analysis, confirmed HDACi-mediated increase in H3K27ac global levels (Fig. 3A-C, S3A). Interestingly, treatment with Sulfopin alone had the opposite effect, reducing the percentage of acetylated nucleosomes (Fig. 3B-C, S3A). As acetylation is coupled with transcription activation, this is in line with the function of Sulfopin as an inhibitor of MYC transcriptional activity[26,61]. As a result, the global HDACi-mediated increase in histone acetylation was also attenuated in the combined treatment with Sulfopin (Fig. 3B-C, S3A).

To profile changes in the genomic distribution of H3K27ac and H3K27me3, we applied Cut&Run in SU-DIPG13 cells treated with Vorinostat alone or in combination with Sulfopin.

193 We first examined the promoters of genes differentially expressed in the combined treatment
194 (as clustered in Fig. 2G). Genes comprising cluster 1 showed higher basal expression levels
195 compared to genes from cluster 4, and these expression differences were also reflected in higher
196 H3K27ac at these genes' promoters (Fig. S3B-C). Moreover, in accordance with the reduction
197 in RNA expression levels of genes comprising cluster 1, the combined treatment led to the
198 strongest local reduction of H3K27ac levels associated with their promoters (Fig. 3D).
199 Specifically, we found that several of the oncogenes that comprise cluster 1, such as mTOR,
200 and mTOR regulator-SLC7A5, RELB and COPB2, showed decreased levels of H3K27ac at
201 their promoters following the combined treatment[62–64] (Fig. 3E, S3D). Cluster 1 genes also
202 gained H3K27me3 on their promoters upon the combined treatment, supporting their epigenetic
203 repression following Sulfopin and Vorinostat treatment (Fig. S3E).

204 We further identified genomic regions in which histone acetylation is lost in a Sulfopin-
205 dependent manner (i.e., H3K27ac peaks that are present in Vorinostat-treated cells, but are lost
206 in the combined treatment with Sulfopin). Genome distribution analysis of these unique peaks
207 revealed that the majority of them localize to distal regions (Fig. S3F) and more than 60% of
208 them localize to annotated enhancers. Importantly, genes associated with these enhancers were
209 strongly enriched for oncogenic pathways such as RAS, MAPK and PI3K-AKT signaling
210 pathways[66–68] (Fig. 3F, S3G). Specifically, the combined treatment reduced H3K27ac levels on
211 several enhancers linked to genes involved in mTOR pathway and gliomagenesis, such as:
212 *AKT3*, *JAK1* and *NFKB2* genes, that were shown to have critical role in malignant gliomas[69–
213 73], *SEC13* gene that indirectly activates mTOR[74,75], and *CD93*, a key regulator in glioma[76] (Fig
214 3G and S3H). Concomitant with the lower H3K27ac levels associated with these enhancers, we
215 also observed lower expression of the associated genes (Fig. 3H and S3I). Taken together, the
216 results show attenuation of HDACi-mediated accumulation of H3K27ac levels upon combined
217 treatment with Sulfopin, associated with promoters and enhancers of prominent oncogenes.
218 This is in-line with reduced expression of these oncogenic pathways, strengthening the
219 therapeutic potential of the combined treatment.

220 **The combined treatment reduces tumor growth in a DMG xenograft mouse model**

221 Finally, we examined whether the combined inhibition of HDACs and PIN1 elicits an additive
222 effect also *in-vivo*. Thus, we established a H3-K27M DMG orthotopic xenograft model by
223 injections of SU-DIPG13P* cells, engineered to express firefly luciferase, to the pons of
224 immunodeficient mice[17]. Mice were given ten days to develop tumors, and then randomly
225 assigned to four groups: control mice treated with DMSO, mice treated with Sulfopin or
226 Vorinostat as single agents, and mice treated with the combination of Sulfopin and Vorinostat.
227 Tumor growth was monitored by in *in-vivo* bioluminescence imaging. In-line with our *in-vitro*
228 results, we found significant reduction in tumor growth following the combined treatment

229 compared to control DMSO treated mice (Fig. 4A-B). Importantly, the reduction was also seen
230 when comparing to mice treated solely with Vorinostat, supporting the additive value of
231 Sulfopin to the well-known anti-tumorigenic effect of HDACi in H3-K27M gliomas[17] (Fig. 4A-
232 B). Of note, mice from all groups showed signs of severe dehydration and general deterioration
233 after 18 days of treatment, and thus we could not measure a survival benefit for the combined
234 treatment.

235 To link our *in-vitro* transcriptomic analysis to the *in-vivo* effect on tumor growth, we assessed
236 the percentage of H3-K27M cells that are positive to mTOR signal (double-positive), out of the
237 total number of H3-K27M cells, by immunofluorescence staining. The combined treatment
238 significantly reduced the fraction of the double-positive cells, compared to DMSO (Fig. 4C-D).
239 Of note, mTOR signal in the mouse cells surrounding the tumor showed no significant
240 differences between the DMSO and the combination-treated mice (Fig S4A-B). Overall, these
241 results verify the potency of this treatment in restricting oncogenic pathways also *in-vivo*, and
242 the potential clinical benefit of PIN1 and HDAC combined inhibition in H3-K27M-mutant
243 DMGs.

244 **Discussion**

245 Despite decades of efforts to improve treatment for children diagnosed with H3-K27M-mutant
246 DMGs, the standard of care remains solely radiation, with no significant improvement in
247 overall survival[1,2,79]. High throughput drug screens in patient-derived cells identified HDAC
248 inhibition as a promising therapeutic strategy, and ongoing clinical trials revealed preliminary
249 evidence of clinical benefit[38,80] (NCT02717455, NCT03566199). However, emerging
250 resistance to HDACi in glioma cells[17], as well as limited therapeutic benefits of HDACi
251 treatment as a sole agent[81,82], highlight the necessity to discover additional therapy modalities
252 that could prolong survival and relieve symptoms.

253 In H3-K27M-mutant DMGs, as well as in many other malignancies, high MYC activity is
254 correlated with poor prognosis and therefore considered as an attractive therapeutic target[21,83].
255 Nevertheless, direct targeting of MYC is highly challenging, functional and structural wise.
256 MYC signaling, while amplified in cancer cells, is also essential to normal cell function[84].
257 Moreover, as a transcription factor, MYC lacks traditionally druggable binding pockets,
258 hindering the development of direct small molecule binders[25]. To overcome this, in this study
259 we exploited Sulfopin, a novel, potent and selective PIN1 inhibitor[26]. Pre-clinical studies have
260 shown *in-vivo* activity and negligible toxicity of Sulfopin in murine models of PDAC and
261 neuroblastoma[26]. While PIN1 is not overexpressed in DMG tumors, we show that Sulfopin,
262 although not inhibiting MYC directly, downregulates MYC target genes in patient-derived
263 DMG cells and affects cell survival in a H3-K27M-dependant manner. These results are in line

264 with the contribution of MYC signaling to H3-K27M-driven tumorigenesis[23,24], underscoring
265 the therapeutic potential of Sulfopin for these aggressive brain tumors. Notably, despite a
266 significant reduction in tumor size *in-vivo*, the combined treatment did not increase mice
267 survival. This is perhaps due to the relatively large tumors already formed at the onset of
268 treatment, pointing to the need for further optimization of the therapeutic regime.

269 We showed that combining Sulfopin treatment with the HDAC inhibitor Vorinostat reduced
270 cell viability by 80% in several tumor-derived DMG lines originating from different patients.
271 Importantly, the combination resulted in an additive effect not only on cell viability, but also
272 on transcriptional programs. A key oncogenic pathway that was robustly downregulated in the
273 combined treatment, *in-vitro* and *in-vivo,* is the mTOR signaling pathway. Preclinical and
274 clinical data support a role for mTOR in gliomagenesis[85]. Specifically, AKT gain or PTEN loss
275 is detected in approximately 70% of DMG tumors, and a recent study showed high expression
276 of mTOR in DMGs. Thus, the PTEN/AKT/mTOR pathway is suggested to play a key role in
277 this disease[86–89]. Attempts to restrict mTOR signaling using first generation mTOR inhibitors
278 primarily inhibited mTORC1, which often caused upregulation of mTORC2[90]. The combined
279 treatment with Sulfopin and Vorinostat led to robust inhibition of several target proteins in the
280 mTOR signaling pathway, likely via alternative pathways. One potential candidate is the
281 mTOR-dependent cell-growth through MYC regulation, which may be impaired by Sulfopin
282 treatment, inhibiting MYC transcriptional activity[91–94]. Of note, drug agents targeting both
283 mTORC1 and mTORC2 were shown to be highly effective in DMG cells as well as in murine
284 models[95,96].

285 Expression of the H3-K27M oncohistone is associated with a prominent increase in H3K27ac
286 levels[11–13,16]. Among the loci that accumulate this modification are repetitive elements and
287 endogenous retroviruses (ERVs), resulting in their aberrant expression, potentially inducing
288 innate immune responses[12]. However, H3-K27M cells do not show an increase in interferon
289 stimulated genes (ISGs), preassembly due to high levels of MYC, which is potent antagonist of
290 interferon responses[12,97]. Thus, dual targeting of both HDAC and MYC pathways has the
291 potential of inducing robust expression of ISGs, thus promoting tumor cell death mediated by
292 viral-mimicry[98].

293 The high levels of H3K27ac in H3-K27M cells was also linked to activation of super-enhancers,
294 which regulate the expression of oncogenes and genes that are associated with an
295 undifferentiated state[79]. Here, we show that H3-K27M cells are vulnerable to transcriptional
296 disruption mediated by the combined treatment with Sulfopin and Vorinostat. While treating
297 cells with Vorinostat alone increased H3K27ac levels, as expected, the combined treatment
298 attenuated the accumulation of this mark on promoters and enhancers of prominent oncogenes,
299 resulting in their decreased expression. This Sulfopin-mediated attenuation could potentially

result from downregulation of MYC targets, as it was recently shown that MYC overexpression results in H3K27ac gain on super-enhancers[99].

In summary, we propose a novel therapeutic strategy targeting epigenetic and transcriptional pathways in H3-K27M-mutant DMG tumors. HDAC inhibition, in combination with the novel MYC inhibitor, inhibited oncogenic transcriptional signatures and reduced tumor growth *in-vivo*. Our findings emphasize epigenetic dependencies of H3-K27M driven gliomas and highlight the therapeutic potential of combined treatments for this aggressive malignancy.

Acknowledgments

We thank H. Keren-Shaul, D. Robbins, Y. Elazari and N. Adler (G-INCPM, WIS) for their help with NGS; N. Morris for her help with conducting part of the cell viability assays; C. Raanan, and M. Zerbib for their contribution in establishing the DIPG mouse model; I. Savchenko for his help with immunohistochemistry; R. Gabizon for generously providing Sulfopin for *in-vitro* and *in-vivo* experiments and helping with Sulfopin handling; S. Fishilevich for providing the GeneHancers data; L. Segev for computational framework for single-molecule image analysis; N. Harpaz and O. Beresh for helping with cultures maintenance; O. Griess for helping with transcriptomic protocols; S. Gillespie for providing valid information on DMG cells growth and maintenance; and I. Ulitsky for providing the pAG-MNase enzyme. We are thankful to O. Golani for helping with the immunohistochemistry image analysis. We are grateful to M. Monje for generously sharing with us the SU-DIPG13, SU-DIPG13P*, SU-DIPG6, SU-DIPG17, SU-DIPG25, SU-DIPG36, SU-DIPG38, SU-DIPG21 and SU-DIPG50 cells. We are grateful to N. Jabado for her kind gift of the isogenic BT245 and SU-DIPG13 cultures. We would like to express our sincere gratitude to D. Deitch for producing part of the graphs, designing the figures and illustrations, and helping with statistical analysis. **Funding:** E.S. is an incumbent of the Lisa and Jeffrey Aronin Family Career Development chair and is also supported by Henry Chanoch Krenter Institute for Biomedical Imaging and Genomics. This research was supported by grants from the European Research Council (ERC801655), The Israel Science Foundation (1881/19), Emerson Collective, and The Israel Cancer Research Fund: Research Career Development Award.

Author contributions

D.A, N.F and E.S. designed the study and wrote the manuscript; D.A conducted the experiments; R.O and A.H established the xenograft mice model and performed *in-vivo* experiments; B.D, D.A, N.F and E.S performed bioinformatics analysis. L.F.A, R.O, G.R and D.A conducted the *in-vivo* image analysis; H.B and A.P conducted part of the viability assays; N.L suggested and provided Sulfopin and valuable usage information.

Declaration of interests

335 N.L. is an inventor on a patent describing Sulfopin (US 2021/0332024 A1).

336 **Figure legends**

337 **Figure 1: Sulfopin inhibits MYC signaling and reduces viability of DMG cells in a H3-**
338 **K27M-dependent manner**

339 (A) Functional enrichment analysis on significantly downregulated genes in SU-DIPG13 cells
340 treated with 10uM Sulfopin for 12 hours, compared to DMSO. Enrichr algorithm[123] was used
341 to compare downregulated genes against the Molecular Signatures Database (MSigDB)
342 hallmark geneset[119]. Dashed line denotes adjusted p-value = 0.05. MYC targets are significantly
343 enriched among the Sulfopin downregulated genes.

344 (B) RT-qPCR analysis of selected MYC target genes in SU-DIPG13 cells treated with 10uM
345 Sulfopin for 12 hours, compared to DMSO. Fold change between Sulfopin and DMSO treated
346 cells was calculated and the mean ± SD of two technical repeats is shown.

347 (C) H3K27me3 Cut&Run read coverage over MYC target genes ('MYC Targets V1' hallmark
348 geneset[119], n=200), in SU-DIPG13 cells treated with 10uM Sulfopin for 8 days compared to
349 DMSO. Sulfopin treatment increases H3K27me3 levels on the TSS of MYC target genes.

350 (D) Functional enrichment analysis of the genes associated with Sulfopin-unique H3K27me3
351 peaks, in SU-DIPG13 cells treated as in C. Dashed line denotes adjusted p-value = 0.05. MYC
352 target geneset ('MYC Targets V1' hallmark geneset[119]) is mildly enriched among these genes,
353 with adjusted p-value of 0.077.

354 (E) Cell viability, as measured by CellTiterGlo, of eight DMG cultures (H3.3K27M: SU-
355 DIPG13, SU-DIPG6, SU-DIPG17, SU-DIPG25 and SU-DIPG50. H3.1K27M: SU-DIPG36,
356 SU-DIPG38 and SU-DIPG21), treated with Sulfopin for eight days with pulse at day four,
357 compared to DMSO. Mean±SD of two technical replicates is shown. Logarithmic scale is used
358 for the x-axis. Sulfopin treatment led to a mild reduction in cell viability in all H3-K27M glioma
359 cultures.

360 (F) Cell viability, as measured by CellTiterGlo, of two isogenic DMG cell lines (SU-DIPG13
361 and BT245) in which the mutant histone was knocked-out (KO), treated with the indicated
362 concentration of Sulfopin for 8 days, compared to DMSO. For each cell line and concentration,
363 the fold change in viability between Sulfopin and DMSO treated cells is shown. For SU-
364 DIPG13-mean ± SE of at least two independent experiments is shown. For BT245-mean± SD
365 of three technical replicates is shown. H3-K27M glioma cells show higher sensitivity to
366 Sulfopin treatment compared to the KO cells. *P < 0.05; **P < 0.01 (two-sample t-test over all
367 technical replicates). Significance adjusted after Bonferroni correction.

368

369 **Figure 2: Combination of Sulfopin and Vorinostat elicits robust downregulation of**
370 **oncogenic pathways**

371 (A) Timeline demonstrating the treatment protocol for the combination of Sulfopin and
372 Vorinostat.

373 (B) Percentage of cell viability, as measured by CellTiterGlo of SU-DIPG13 cells treated with
374 Sulfopin and Vorinostat at the indicated concentrations, compared to DMSO.

375 (C) BLISS index measured as the ratio between the observed and the expected effect of the
376 combination of Sulfopin and Vorinostat, for each pair of concentrations, in SU-DIPG13.
377 Synergy: Bliss <1 ,Additive: Bliss=1, Antagonist: Bliss>1.

378 (D) Cell viability as measured by CellTiterGlo, of eight DMG cultures treated with Sulfopin
379 (0uM, 2.5uM, 5uM, 10uM, 20uM and 40uM) and Vorinostat (1uM), compared to DMSO.
380 H3.3-K27M and H3.1-K27M cultures are indicated in blue and orange, respectively. Mean±SD
381 of two technical replicates is shown. H3.3-K27M cells showed higher sensitivity to the
382 combined treatment compared to H3.1-K27M cells.

383 (E) The BLISS index of the combination of Sulfopin (10uM) and Vorinostat (1uM), in the
384 indicated cultures. An additive effect was detected in all the H3.3-K27M cultures at this set of
385 concentrations.

386 (F) Pearson correlation coefficient matrix of BLISS index of the combined treatment (Sulfopin
387 (10uM) and Vorinostat (1uM)) and mRNA levels of MYC and its target genes, in the eight
388 DMG cultures tested. mRNA levels were measured by RT-qPCR (Fig. S2F-G). Blue and yellow
389 colors indicate negative or positive correlation, respectively. Negative correlation was detected
390 between the BLISS indexes and the expression levels of MYC and its target genes.

391 (G) Unsupervised hierarchical clustering of expression levels of 620 significantly DE genes
392 detected in SU-DIPG13 cells treated with either Sulfopin (10uM, 8 days), Vorinostat (1uM, 72
393 hours), the combination of Sulfopin and Vorinostat or DMSO. Gene expression rld values (log2
394 transformed and normalized) were standardized for each gene (row) across all samples. Color
395 intensity corresponds to the standardized expression, low (blue) to high (red). Clusters 1 and 4
396 demonstrate additive transcriptional patterns associated with the combined treatment.

397 (H) Top: Gene Set Enrichment Analysis (GSEA) on SU-DIPG13 treated with combination of
398 10uM Sulfopin and 1uM Vorinostat compared to DMSO, showing significant downregulation
399 of mTORC1 signaling ('HALLMARK_MTORC1_SIGNALING' geneset[119]) in the combined
400 treatment. NES: Normalized Enrichment Score. FDR: false discovery rate. Bottom: Expression
401 levels of significantly DE genes detected in the combined treatment compared to DMSO that

402 are part of the mTORC1 signaling geneset. *MTOR* gene was added manually to the heat-map.
403 Heatmaps were generated as described in B.

404 (I) Top: Gene Set Enrichment Analysis (GSEA) on SU-DIPG13 treated as in C, showing
405 significant downregulation of the epigenetic BMI-1 pathway and the oncogenic cAMP pathway
406 in the combined treatment (BMI1_DN.V1_UP; CAMP_UP.V1_UP; MSigDB C6 oncogenic
407 signature[120,121]). Bottom: Expression levels of significantly DE genes detected in the combined
408 treatment compared to DMSO that are part of the BMI-1 and cAMP genesets. Heatmaps were
409 generated as in described B.

410 (J) Western blot of SU-DIPG13 treated either with Sulfopin (10uM, 8 days), Vorinostat (1uM,
411 72 hours), the combination of Sulfopin and Vorinostat or DMSO, using the indicated
412 antibodies. β-tubulin is used as loading control.

413

414 **Figure 3: The combined treatment attenuates H3K27ac levels on oncogenic targets**

415 (A) Scheme of the single-molecule imaging experimental setup[133]: cell-derived mono-
416 nucleosomes are anchored in a spatially distributed manner on polyethylene glycol (PEG)-
417 coated surface. Captured nucleosomes are incubated with fluorescently labeled antibodies
418 directed against the H3K27ac modification. Total internal reflection fluorescence (TIRF)
419 microscopy is utilized to record the position and modification state of each nucleosome. Time
420 series images are taken to allow detection of maximal binding events.

421 (B) Single-molecule imaging quantification of the percentage of H3K27ac nucleosomes, in SU-
422 DIPG13 cells treated with either Sulfopin (10uM, 8 days), Vorinostat (1uM, 72 hours), or the
423 combination of Sulfopin and Vorinostat, normalized to DMSO. Mean fold ± SE of at least two
424 independent experiments is shown. H3K27ac global levels are lower in the combined treatment
425 compared to cells treated solely with Vorinostat. *$P < 0.05$ (two sample t-test).

426 (C) SU-DIPG13 cells were treated as in B, and analyzed by western blot using the indicated
427 antibodies.

428 (D) Left panel: Heatmap shows H3K27ac read coverage around the TSS (+/-5Kb) of the
429 significantly DE genes shown in figure 2B, in SU-DIPG13 cells treated with the combination
430 of 10uM Sulfopin and 1uM Vorinostat versus DMSO. Average coverage is shown on top. Color
431 intensity corresponds to the standardized expression. Clusters 1-4 are indicated. Right panel:
432 The log2 ratio of H3K27ac read coverage in SU-DIPG13 cells treated with the combination of
433 10uM Sulfopin and 1uM Vorinostat vs. DMSO was calculated. Heatmap shows the ratio around
434 the TSS (+/-5Kb) of the significantly DE genes shown in figure 2B, and average coverage is
435 shown on top. Color intensity corresponds to the ratio between samples, low (red) to high
436 (blue). Clusters 1-4 are indicated, with cluster 1 presenting the strongest local decrease in
437 H3K27ac following the combined treatment compared to DMSO.

438 (E) IGV tracks of *MTOR* and *SLC7A5* gene promoters, showing H3K27ac coverage in SU-
439 DIPG13 cells treated as indicated.

440 (F) Functional enrichment analysis of the genes linked to enhancers (top targets of high
441 confident enhancers) marked with H3K27ac exclusively in SU-DIPG13 cells treated with
442 Vorinostat, and not in the combined treatment. gProfiler algorithm[126] was used to calculate
443 enrichment against the KEGG pathways DB[128]. Dashed line denotes adjusted p-value = 0.05.
444 Genes associated with Vorinostat-unique enhancers are enriched for oncogenic signaling
445 pathways.

446 (G) IGV track of *AKT3* and *SEC13* linked enhancers, showing H3K27ac coverage in SU-
447 DIPG13 cells treated with 1uM Vorinostat or the combination of 10uM Sulfopin and 1uM
448 Vorinostat.

449 (H) Normalized expression levels of *AKT3* and *SEC13* genes in SU-DIPG13 cells treated as in
450 G. Mean ± SD of three technical repeats is shown .*$P < 0.05$ (two-sample t-test).

451

452 **Figure 4: The combined treatment with Sulfopin and Vorinostat reduces tumor growth**
453 ***in-vivo***

454 (A-B) SU-DIPG13P* cells were injected to the pons of immunodeficient mice to form tumors.
455 Ten days post injection, mice were treated for 18 days with either DMSO, Sulfopin, Vorinostat,
456 or the combination of Sulfopin and Vorinostat. (A) *In-vivo* bioluminescent imaging of DMG
457 xenografts following 18 days of treatment. The heat map superimposed over the mouse head
458 represents the degree of photon emission by DMG cells expressing firefly luciferase. (B) DMG
459 xenograft tumor growth as measured by change in bioluminescent photon emission following
460 15 days of treatment with either DMSO (n=8), Sulfopin (n=4), Vorinostat (n=5) or the
461 combination of Sulfopin and Vorinostat (n=6). Data points represent the fold-change in
462 maximum photon flux between day 3 and day 18 under treatment for each mouse. *$P < 0.05$
463 (two-tailed Mann-Whitney U-test).

464 (C-D) Immunofluorescent staining of brain sections from mice treated with DMSO (n=4) or
465 the combination of Sulfopin and Vorinostat (n=4). (C) Representative fluorescence images of
466 H3-K27M (red) and mTOR (green). (D) Percentage of mTOR positive cells out of the total H3-
467 K27M-positive cells. H3-K27M positive cells show lower levels of mTOR following the
468 combined treatment compared to DMSO. *$P < 0.05$ (two-tailed t-test).

Methods

Data availability

All sequencing data is deposited in NCBI's Gene Expression Omnibus (GEO) and available through GEO series accession number GSE221614.

Cell cultures

All cell lines were maintained at 37°C with 5% CO2. Exclusion of Mycoplasma contamination was monitored and conducted by test with EZ-PCR kit (Biological Industries # 20-700-20).

Glioma cultures

DIPG derived cells, SU-DIPG13 (H3.3-K27M, female), SU-DIPG6 (H3.3-K27M, female), SU-DIPG17 (H3.3-K27M, male), SU-DIPG25 (H3.3-K27M, female), SU-DIPG50 (H3.3-K27M, sex unknown), SU-DIPG36 (H3.1-K27M, female), SU-DIPG38 (H3.1-K27M, female), SU-DIPG21 (H3.1-K27M, male) and SU-DIPG13P* were generated in the lab of Dr. Michelle Monje, Stanford University[17]. SU-DIPG13P* are a subclone of the patient-derived SU-DIPG13 pons culture that demonstrates more aggressive growth in vivo[38,79].

K27M-KO SU-DIPG13, BT245-KO (sex information is unavailable) and corresponding control clones were generated in the lab of Prof. Nada Jabado, McGill University, as previously described by Krug et al[12].

Cells were cultured in Tumor Stem Media (TSM) consisting of a 1:1 mixture of DMEM/F12 (Invitrogen, 31330038) and Neurobasal -A (Invitrogen, 10888022) media, with 1:100 addition of HEPES Buffer Solution (Invitrogen 15630-080), MEM Sodium Pyruvate Solution (Invitrogen, 11360-070), MEM Non-Essential Amino Acids Solution (Invitrogen, 11140-050), GlutaMAX-I (Invitrogen, 35050-061) and Antibiotic-Antimycotic (Invitrogen,15240-096). The following additive were added freshly: B27 -A (1:50, Invitrogen, 12587010), human FGF (20 ng/ml, Shenandoah Biotechnology, 100-146), human EGF (20 ng/ml, Shenandoah Biotechnology, 100-26), human PDGF-AA (20 ng/ml, Shenandoah Biotechnology, 100-16), human PDGF-BB (20 ng/ml, 100-18, Shenandoah Biotechnology) and heparin (10 ng/ml, Stemcell Technologies, 07980). Doubling times were computed using: http://www.doubling-time.com/compute.php.

Astrocytic-like cells culture

CRL-1718 cells, an astrocytic-like cells isolated from the brain of patient with astrocytoma were kindly provided by Dr. D. Michaelson, Tel-Aviv University, Israel. Cells were cultured in RPMI media (Biological Industries, # 01-101-1A) supplemented with 10% heat inactivated

502 Fetal Bovine Serum (FBS), 1 mM L-glutamine and 1% penicillin/streptomycin solution (all
503 from Biological Industries).

504 **Isolation of total RNA, reverse transcription and RT-qPCR**

505 RNA was isolated from 2 million cells using the NucleoSpin kit (Macherey Nagel,
506 #740955.50). 1ug of each RNA sample was reverse-transcribed using Moloney Murine
507 Leukemia Virus reverse transcriptase (M-MLV-RT, Promega, #M1701) and random hexamer
508 primers (Thermo Scientific, #SO142). Real-time qPCR was performed using KAPA SYBR
509 FAST mix (Kapa Biosystems, #KK4660) with a StepOne real-time PCR instrument (Applied
510 Biosystems). For each gene, standard curve was determined and the relative quantity was
511 normalized to GAPDH mRNA (Table S2).

512 **Isolation of total RNA, bulk MARS-Seq library preparation and sequencing**

513 RNA was isolated from SU-DIPG cells treated as indicated in Table S4a, using the NucleoSpin
514 kit (Macherey Nagel, 740955). A bulk adaptation of the MARS-Seq protocol[100,101] was used to
515 generate RNA-Seq libraries for expression profiling. Briefly, 30 ng of input RNA from each
516 sample was barcoded during reverse transcription and pooled. Following Agencourct Ampure
517 XP beads cleanup (Beckman Coulter, A63880), the pooled samples underwent second strand
518 synthesis and were linearly amplified by T7 in vitro transcription. The resulting RNA was
519 fragmented and converted into a sequencing-ready library by tagging the samples with Illumina
520 sequences during ligation, RT, and PCR. Libraries were quantified by Qubit (ThermoFisher
521 Scientific) and TapeStation (Agilent) as well as by qPCR for GAPDH housekeeping gene as
522 described below. Sequencing was done on a Nextseq 75 cycles high output kit (Illumina,
523 20024906).

524 **Bulk MARS-seq analysis**

525 A median of 10.5 to 20 million reads were obtained for each dataset (Table S4a). MARS-seq
526 analysis was preformed using the UTAP transcriptome analysis pipeline[113]. Reads were
527 trimmed to remove adapters and low quality bases using cutadapt[105] and mapped to the human
528 genome (hg38, UCSC) using STAR v2.4.2a18[114] (parameters: –alignEndsType EndToEnd, –
529 outFilterMismatchNoverLmax 0.05, –twopassMode Basic, –alignSoftClipAtReferenceEnds
530 No). In short, the pipeline quantifies the 3' of annotated genes (The 3' region contains 1,000
531 bases upstream of the 3' end and 100 bases downstream). Counting was done using HTSeq-
532 count in union mode[115]. Genes having a minimum 5 UMI-corrected reads in at least one sample,
533 were considered. Normalization of the counts and differential expression analysis was done
534 using DESeq2[116], and is provided in Table S4b-c (parameters: betaPrior=True,
535 cooksCutoff=FALSE, independentFiltering=FALSE). Significantly differentially expressed
536 genes were defined having adjusted p-value (with Benjamini and Hochberg procedure) <= 0.05,

537 |log2FoldChange| >= 1 and baseMean >= 5. Heatmaps of gene expression were calculated using
538 the log-normalized expression values (rld), with row standardization (scaling the mean of a row
539 to zero, with standard deviation of 1). Clustering of gene expression (rld values) was done using
540 Euclidian average linkage method, and visualized using Partek Genomics Suite 7.0 software
541 (Partek Inc. 2020. Partek® Genomics Suite®, Version 7.0). Boxplot was used to visualize gene
542 expression values (rld) of each differentially expressed gene from clusters 1 and 4 (in each of
543 the three replicates).

544 **Expression analysis from published data-sets**

545 Gene expression data and histone mutation status of pediatric high grade gliomas[22] was
546 downloaded from PedcBioPortal (https://pedcbioportal.kidsfirstdrc.org/). For matched tumor-
547 normal samples, RPKM values were obtain from Berlow et al[35] (S2_Table). For boxplots the
548 log2 (RPKM+1) or z-score values were used (ggpubr R package). Differences between groups
549 were assessed using two-sided 't_test' (rstatix R package). For heatmaps, gene expression
550 values were obtained for genes from MsigDB signatures
551 'HALLMARK_MYC_TARGETS_V1', with MYC and PIN1 genes added manually.
552 Heatmaps of gene expression were calculated using RPKM values, with row standardization
553 (scaling the mean of a row to zero, with standard deviation of 1).

554 **Functional enrichment analysis**

555 Gene set enrichment analysis (GSEA) was performed as described in
556 www.broadinstitute.org/software/gsea[117,118]. Genes detected by MARS-seq were pre-ranked
557 according to their fold change (log2) in Sulfopin+Vorinostat vs. DMSO treated cells. Pre-
558 ranked GSEA was applied using the Human MSigDB Collections H: hallmark gene sets[119], and
559 the C6: oncogenic signature gene sets[120–122]. Significantly downregulated gene-sets were
560 selected using cut-off of FDR q-value ≤ 0.1.

561 Enrichr algorithm[123] was used to compare significantly downregulated genes detected in the
562 different treatments, against one or more of the following databases: the Molecular Signatures
563 Database (MSigDB) hallmark[119], ChEA[124] or ENCODE TF ChIP[125].

564 gProfiler algorithm[126] was used to analyze genes that are putative targets of elite enhancers
565 which overlap with Vorinostat-unique H3K27ac peaks (see Cut&Run analysis), against the
566 KEGG[127,128] or Wiki[129] pathways databases.

567 **Cut&Run pulldown assay followed by high-throughput sequencing**

568 Cut&Run assay was done as described in Skene and Henikoff, 2017[31,102] with slight
569 modifications as follows: Cells were harvested and counted, with 200,000 cells taken per
570 reaction. Permeabilized cells, bound to Concanavalin A-coated beads (Bangs Laboratories,

571 BP531), were mixed with individual primary antibody (Table S1) and incubated overnight at
572 4°C while rotating. Secondary antibody, anti-rabbit HRP, was used as a negative control. pAG-
573 MNase enzyme (generated in the Department of Life Sciences Core Facilities, WIS, using
574 Addgene plasmid 123461) was added to each sample followed by incubation step of 1 h at 4°C.
575 Targeted digestion was done by 15 min incubation on ice block (0°C) under low salt conditions.
576 DNA purification was done using Nucleospin gel and PCR clean-up kit (Machery-Nagel,
577 740609).

578 Libraries were prepared from 1-20ng of DNA as previously described in Blecher-Gonen et al[103].
579 Briefly, DNA Fragments were repaired by T4 DNA polymerase (NEB, M0203), and T4
580 polynucleotide kinase (T4 PNK, NEB, M0201) was used to add a phosphate group at the 5′
581 ends. An adenosine base was then added by Klenow fragments (NEB, M0212) to allow efficient
582 ligation, using T4 quick ligase (NEB, M2200), of sequencing adapters, which contain a T-
583 overhang. DNA fragments were amplified by PCR reaction (Pfu Ultra II fusion, Agilent
584 Technologies, 600670), which also introduced the Illumina-P5 adapter at one end of the
585 molecule. SPRI beads were used to purify proper sized DNA fragments after each enzymatic
586 step. Libraries were quantified by Qubit (ThermoFisher Scientific) and proper fragment range
587 (200-400bp) was verified by TapeStation (Agilent). Sequencing was done on a Next-Seq 500
588 instrument (Illumina, #20024904) using a V2 150 cycles mid output kit (paired end
589 sequencing).

590 Paired-end reads of each sample (~7.5M median reads per sample, Table S5) were preprocessed
591 with cutadapt[105], to remove adapters and low-quality bases (parameters: --times 2 -q 30 -m 20),
592 following evaluation of quality with FastQC. Reads were mapped to human genome (hg38,
593 UCSC) using Bowtie version 2.3.5.1[106] (--local --very-sensitive-local --no-unal --no-mixed --
594 no-discordant --dovetail -I 10 -X 700). Nucleosome fragments at the length >120bp were
595 selected from the remaining unique reads using picard-tools, and broad peaks were called using
596 MACS2 against the HRP samples as background control (parameters: -f BAMPE --SPMR --
597 nomodel --extsize 100 --keep-dup auto -q 0.05). Analysis of genomic features was done using
598 ChIPseeker[107]. Reads coverage on TSS, gene body regions, specific gene-signatures and CGI
599 were visualized using ngs.plot[108]. Annotation of CGI were downloaded for UCSC table
600 browser. Association of peaks with specific genes was done using GREAT[109]. Bigwig files
601 were constructed from BAM alignments using deepTools2 suite[110], by 'bamCoverage'
602 command, using RPKM-normalization in 10bp bins. Heatmaps and profiles were constructed
603 in 'scale-regions' mode around peak summits, with missingDataAsZero paramter using
604 'plotHeatmap' and 'plotProfile' commands. In the heatmap of H3K27ac ratio (Fig. 3D)
605 coverage was calculated as the log2 between treatment and DMSO, on TSS of genes which
606 were depicted as differentially expressed by MARS-Seq. RPKM-normalized coverage files

607 were visualized on the genome using IGV (2.8.6). H3K27ac peaks were further distinguished
608 into Vorinostat-unique peaks (i.e., H3K27ac peaks that are present in Vorinostat-treated cells,
609 but are lost in the combined treatment with Sulfopin), and to shared peaks (i.e., H3K27ac peaks
610 that are present both in Vorinostat and in Sulfopin+Vorinostat treated cells, with a minimum of
611 1bp overlap) using bedtools[111]. H3K27me3 peaks unique to Sulfopin treatment were defined
612 similarly. To detect the overlap between the Vorinostat-unique peaks with enhancer regions,
613 we used the GeneHancer database v5.9[112]. We required a 30% overlap of the peak length with
614 a known enhancer categorized as "Elite" group, and excluded enhancers annotated to promoters
615 regions.

616 **Cell viability assay by CelltiterGlo**

617 For Sulfopin and Vorinostat combination experiments, 384-well plates were pre-plated with 2-
618 fold dilution matrix of Vorinostat (MCE Cat#HY-10221) and Sulfopin (generous gift from Dr.
619 Nir London's Lab, Weizmann institute of science), in 5 concentrations ranging from 120 to
620 10,000 nM (Vorinostat) and 2500 to 40,000 nM (Sulfopin). 1400 DIPG cells/well were plated
621 into each well containing 75ul of growth media, and subjected to drug treatment for 3 days
622 (Vorinostat) or 8 days with pulse at day 4 (Sulfopin). Single agent titrations were run in parallel.
623 Following the treatment, cells were subjected to cell viability assay using CellTiter-Glo assay
624 (# G7572, Promega, USA) in accordance to the manufacture protocol. Luminescence signal
625 was detected by luminescence module of PheraStar FS plate reader (BMG Labtech, Ortenberg,
626 Germany). Viability data was analyzed using GeneData 15 (Switzerland).

627 For generating Sulfopin dosage curves in DIPG versus Astrocytes cells, the appropriated
628 amounts of Sulfopin or DMSO (control) were transferred using Echo Liquid Handler 550
629 (Beckman, USA) into white/white 384-well TC plate (Greiner, #781080). 1400 cells/well were
630 dispensed by MultiDrop 384 dispenser (Thermo Scientific, USA) into 384-well plates. After 4
631 days, cells were subjected to cell viability assay using CellTiter-Glo assay (# G7572, Promega,
632 USA) in accordance to the manufacture protocol. Luminescence signal was detected by
633 luminescence module of PheraStar FS plate reader (BMG Labtech, Ortenberg, Germany).
634 Viability data was analyzed using GeneData 15 (Switzerland).

635 For all the other viability assays, cells were plated at a density of 2500 cells/well in 96-well
636 plates and subjected to drug treatment for 3 days (Vorinostat-MCE Cat#HY-10221, GSK-J4-
637 Selleck Cat#S7070, EPZ-6438-Selleck Cat#S7128) or 8 days (Sulfopin, generous gift from Dr.
638 Nir London's Lab, and MM-102-Selleck Cat#S7265) (Table S3). At least two replicates were
639 measured for each treatment. When treated for 8 days drug was also added at day 4. Cell
640 viability was measured by CelltiterGlo assay (G7571, Promega) according to the

641 manufacturer's instructions. Luminescence was measured by Cytation 5 plate reader and
642 viability was compared to DMSO treated control cells.

643 At least two technical replicates were averaged in each experiment, and mean ± SE of all
644 biological repeats was calculated. Two sample t-test on all technical replicates was used to
645 determine significant difference between the treatments. Bonferroni correction was applied
646 whenever more than two comparisons were made.

647 **IC50 quantification**

648 Sulfopin IC50 values were determined by 4-parameter log-logistic dose response model using
649 SynergyFinder 2.0[130].

650 **BLISS index calculation**

651 The Bliss index was calculated as the ratio between observed effect of combined drug
652 treatment and expected effect (based on the calculated effect of combining single-drug
653 treatment)[45,46]:

654 Bliss index = Observed/Expected = $\frac{J_{AB}}{(J_A \times J_B)}$

655 JA is the effect on growth of drug A only compared to DMSO

656 JB is the effect on growth of drug B only compared to DMSO

657 JAB is the effect on growth of drug A and B together compared to DMSO

658 Synergy: Bliss <1

659 Additive: Bliss=1

660 Antagonist: Blliss>1

661 **Western blot analysis**

662 An equal number of cells from different treatments were suspended in Laemmli sample buffer
663 (Bio-Rad, #1610747) containing 50mM DTT (Promega, #V3151), vortexed and heated up to
664 98°C. Samples were loaded onto Novex WedgeWell 4-20%, Tris-Glycine 4-20% gel
665 (ThermoFisher Scientific, XP04205BOX) and electrophoresis was carried out in TG-SDS
666 buffer (Bio-rad #1610732) for 1-1.5 hours at 120V. After electrophoresis, proteins were
667 transferred to nitrocellulose membranes using transfer kit (Bio-rad, #1704156), followed by
668 brief rinse in TBS (Bio-rad, #1706435) and blocking with 5% (w/v) milk powder in TBST
669 (Tween20-Sigma, #P1379) for 60 minutes. The membranes were then rinsed in TBST and
670 incubated with primary antibodies overnight at 4 °C with gentle rocking. Primary antibodies
671 (Table S1) were diluted according to manufacturer instructions in TBST containing 5% (w/v)
672 milk powder. The following day the membranes were rinsed in TBST, then incubated with

673 HRP-conjugated secondary antibody (Table S1) diluted according to manufacturer instructions
674 in a solution containing 5% (w/v) milk powder in TBST. The membranes were then rinsed in
675 TBST and dipped in an ECL WB Detection Reagent (Bio-rad #1705061) prior to exposure.
676 Membranes were imaged using a Bio-Rad ChemiDoc MP imaging system.

677 **Nucleosome preparation for single-molecule imaging**

678 Nucleosomes for single-molecule imaging were extracted and labeled as described in Furth et
679 al[16]. Briefly, 2–2.5 million cells were collected, washed once with PBS supplemented with
680 protease inhibitors cocktail, 1:100, Sigma P8340), and HDAC inhibitors (20mM Sodium
681 butyrate, Sigma 303410 and 0.1mM Vorinostat V-8477), and then resuspended in 0.05%
682 IGEPAL (Sigma I8896) diluted in PBS (supplemented with inhibitors). Cell pellets were then
683 lysed in parallel to chromatin digestion (100mM Tris-HCl pH 7.5, 300mM NaCl, 2% Triton®
684 X-100, 0.2% sodium deoxycholate, 10mM CaCl2) supplemented with inhibitors and
685 Micrococcal Nuclease (ThermoFisher Scientific, 88216). The suspension was incubated at
686 37°C for 10 min and the MNase reaction was inactivated by addition of EGTA at a final
687 concentration of 20mM. Lysate was clear by centrifugation and nucleosomes were concentrated
688 using an Amicon ultra-4 (Millipore, UFC810024). Inhibitors were supplemented following
689 concentration. Nucleosomes labeling the following reaction was used: NEBuffer™ 2 (NEB
690 B7202), inhibitors (as detailed above, 0.25 mM MnCl2, 33uM fluorescently labeled dATP
691 (Jena Bioscience, NU-1611-Cy3), 33uM biotinylated dUTP (Jena Bioscience, NU-803-BIOX),
692 1.5ul of Klenow Fragment (3'→5′ exo-, NEB, M0212S) and 1.5ul of T4 Polynucleotide Kinase
693 (NEB, M0201L). Samples were incubated at 37°C for 1h and then inactivated by addition of
694 EDTA at a final concentration of 20mM. Nucleosomes were then purified on Performa Spin
695 Columns (EdgeBio, 13266) followed by the addition of inhibitors.

696 **Surface preparation for single-molecule imaging**

697 PEG-biotin microscope slides were prepared as described in Furth et al[16]. Ibidi glass coverslips
698 (25mm×75mm, IBIDI, IBD-10812) were cleaned with (1) ddH2O (3X washes, 5 min
699 sonication, 3X washes), (2) 2% Alconox (Sigma 242985, 20min sonication followed by 5X
700 washes with ddH2O), (3) 100% Acetone (20min sonication followed by 3X washes with
701 ddH2O). Slides were then incubated in 1M KOH solution for 30min while sonicated (Sigma
702 484016), followed by 3X washes with ddH2O. Slides were sonicated for 10 min in 100% HPLC
703 EtOH (J.T baker 8462-25) and then incubated for 24 min in a mixture of 3% 3-
704 Aminopropyltriethoxysilane (ACROS Organics, 430941000) and 5% acetic acid in HPLC
705 EtOH, with 1 min sonication in the middle. Following washes with HPLC EtOH (3X) and
706 ddH2O (3X) slides were dried and mPEG:biotin-PEG solution was applied (20mg Biotin-PEG
707 (Laysan, Biotin-PEG-SVA-5000), 180mg mPEG (Laysan, MPEG-SVA-5000) dissolved in

708 1560ul 0.1M Sodium Bicarbonate (Sigma, S6297) on one surface followed by the assembly of
709 another surface on top. Surfaces were incubated overnight in a dark humid environment and at
710 the following day, were washed with ddH2O and dried. MS (PEG) 4 (ThermoFisher Scientific,
711 TS-22341) was diluted in 0.1M of sodium bicarbonate to a final concentration of 11.7 mg/mL
712 and applied on the surfaces for overnight incubation in dark humid environment. Surfaces were
713 washed with ddH2O and dried.

714 **Single-molecule imaging of histone modifications**

715 PEG-biotin coated coverslips were assembled into Ibidi flowcell (Sticky Slide VI hydrophobic,
716 IBIDI, IBD-80608). Streptavidin (SIGMA, S4762) was added to a final concentration of
717 0.2mg/mL followed by an incubation of 10 min. TetraSpeck beads (used for image alignment,
718 ThermoFisher Scientific, T7279) diluted in PBS were added and incubated on surface for at
719 least 30 min. Labeled nucleosomes were incubated for 10 min in imaging buffer (10mM MES
720 pH 6.5 (Boston Bioproducts Inc, NC9904354), 60mM KCL, 0.32mM EDTA, 3mM MgCl2,
721 10% glycerol, 0.1mg/mL BSA (Sigma, A7906), 0.02% Igepal (Sigma, I8896) to allow
722 immobilization via biotin-streptavidin interactions and washed with imaging buffer. H3K27ac
723 antibody was diluted in imaging buffer (1:2000) and incubated for 30 min. All positions (80–
724 100 fields-of-view (FOV) per experiment) were then imaged by a total internal reflection
725 (TIRF) microscope by Nikon (Ti2 LU-N4 TIRF) every 10 min (10–15 cycles).

726 Image analysis was performed with Cell Profiler image analysis tools
727 (http://www.cellprofiler.org/) as described in Furth et al[16]. Image analysis is done in two steps:
728 (1) Time-lapse images of antibody binding events and TetraSpeck beads are aligned, stacked
729 and summed to one image. Antibody spots and TetraSpeck beads spots were distinguished
730 based on the size of the spot. (2) Stacked images are aligned to the initial images of the
731 nucleosomes based on TetraSpeck beads location spots, and only binding events that align with
732 nucleosomes are filtered and saved for further analysis. To evaluate random co-localization
733 (negative control), each stacked image is aligned to a 90° flipped image of the initial
734 nucleosomes. The use of TetraSpeck beads and a highly accurate microscope stage allowed
735 alignment of images with shifts of up to 30 pixels. Nucleosomes are initially distributed on the
736 surface in low density to minimize overlap between spots. Average percentage of modified
737 nucleosomes over all fields of view (FOV) imaged was calculated in each experiment. Mean ±
738 SE of three to five biological repeats was calculated. Two sample t-test on all biological repeats
739 was used to determine significant difference between the treatments.

740 **Mouse injection and treatment**

741 All animal experiments were conducted in accordance with approved institutional animal care
742 and use committee protocols. Mice were housed and handled in a specific-pathogen-free,

743 temperature-controlled (22°C ± 1°C) mouse facility on a reverse 12/12 h light/dark cycle,
744 Animals were fed a regular chow diet et libitum. Single-cell suspension of SU-DIPG13P* or
745 SU-DIPG13 cells were stereotactically injected into the pons of male NGS mice (NOD-SCID-
746 IL2R gamma chain-deficient, The Jackson Laboratory) as previously described in Venkatesh
747 et al[104]. Injection coordinates were: 0.8 mm posterior to lambda, 1 mm lateral to the sagittal
748 suture, and 5 mm deep. Briefly, the skull of the mouse was exposed, and a small bore hole (0.5
749 mm) was made using a high-speed drill at the appropriate stereotactic coordinates.
750 Approximately 300,000-400,000 cells in 3ul volume were injected at a speed of 0.3ul per
751 minute into the pons with a 26-gauge Hamilton syringe; following 10 min pause, the needle
752 was removed at a speed of 0.2 mm/minute. After closing the scalp, mice were placed on a
753 heating pad and returned to their cages after full recovery. Mice were randomized to treatment
754 groups, and treatment started 10 days (SU-DIPG13P*) or 5 weeks (SU-DIPG13) post-injection.
755 Treatment was given daily for 18 days, by intraperitoneal injection according to the following
756 groups: Vorinostat 200mg/kg daily (LC, V-8477-SU-DIPG13P*; MCE, HY-10221- SU-
757 DIPG13), Sulfopin 40 mg/kg (gift from Dr. Nir London's Lab), combination 200 mg/kg
758 Vorinostst and 40 mg/kg Sulfopin, control mice received solvent 15% DMSO in 50% PEG400
759 (Sigma) in 0.15M NaCl.

760 **Tumor size imaging using IVIS**

761 For bioluminescence imaging, mice received 100 µl D-luciferin (33 mg/ml; Perkin-elmer,
762 Cat#122799) intraperitoneally 10 min before isoflurane anesthesia and were placed in LagoX
763 Imaging System (Spectral Instruments Imaging).

764 The bioluminescence signal was measured using the ROI tool in LagoX software (Spectral
765 Instruments Imaging). The fold change in total Photon flux (p/s) over time was used to compare
766 tumor growth between the groups. Mann-Whitney U-test (Two-tailed) was used to determine
767 significant difference between the DMSO and Sulfopin+Vorinostat treated mice.

768 **Mouse brain slides staining**

769 Brains were collected, fixed in 4% paraformaldehyde, and embedded in paraffin blocks. For
770 H3-K27M and mTOR staining, slides were de-paraffinized (1-Xylene –Bio-lab #242500; 2-
771 Xylene; 3-Eth 100%-Bio-lab #05250501;4- Eth- 96%; 5-Eth-70%;) and incubated in acetone
772 (Bio-lab, #010352) at -20C. Slides were incubated in hydrogen peroxide blocking solution
773 (200ml Methanol-Bio-lab #136805, 1% HCl-Bio-lab #084102, 3% H2O2- JT Baker #2186-01)
774 for blocking endogenous peroxidase activity. Antigen retrieval was performed using citric acid
775 buffer at pH-6, followed by blocking with 20% NHS and 0.5% triton in PBS. Rabbit anti mTOR
776 (1:100, Table S1) was diluted in 2% NHS and 0.5% triton and was incubated overnight at room
777 temperature. Slides were then incubated with HRP conjugated goat anti rabbit (1:100, Table

778 S1) diluted 2% NHS for 1.5hr followed by OPAL 650 (1:500, Akoya FP1496001KT) reagent
779 incubation for 15 min. Antibodies were stripped using microwave treatment with citric acid at
780 pH-6, blocked and again incubated with rabbit anti H3-K27M (1:100 table S1) overnight at
781 room temperature. Slides were then incubated with HRP conjugated goat anti rabbit (1:100,
782 Table S1) diluted 2% NHS for 1.5hr followed by OPAL 570 (1:500, Akoya FP1488001KT)
783 reagent incubation for 15 min. Slides were then washed with PBS and incubated with Hoechst
784 (1:1000) for 1 minutes, followed by mounting with 25x75x1mm glass slides using Aqua-
785 Poly/Mount Mounting Medium. All slides were scanned using the Panoramic MIDI slide
786 scanner (3D Histech, Hungary) at x20 magnification, to receive a full scan of the tumor section.

787 For H3-K27M and mTOR co-localization analysis, double stained cells were counted using
788 ImageJ. First, threshold based segmentation was used to detect positive cells in each of the
789 channels and the image calculator feature was used to find the double positive cells. The total
790 number of double-positive cells was then divided by to total number of H3-K27M-positive cells
791 to calculate the percentage co-localization\H3-K27M cells. For mTOR signal quantification in
792 non-tumor cells (mice cells) a region of interest was selected in a location on the section with
793 no positive H3-K27M cells. Threshold based segmentation was used to detect the percentage
794 mTOR stained area.

795 **Statistical analysis**

796 Unless noted otherwise, p values were determined using two-sample t-test and are indicated in
797 the figure legends.

798 Pearson correlation coefficient was used to assess the relationship between all variables. Scatter
799 plot was generated using ggscatter (R ggpubr package).

800

801 **Supplementary Materials**

802 Figures S1-S4

803 Table S1: Antibodies used throughout the study

804 Table S2: Oligonucleotides used throughout the study

805 Table S3: Drugs and inhibitors used throughout the study

806 Table S4a-c: Summary tables of MARS-seq libraries

807 Table S5: Summary table of Cut&Run libraries

808 **References**

809 1. Johung, T.B., and Monje, M. (2016). Diffuse Intrinsic Pontine Glioma: New
810 Pathophysiological Insights and Emerging Therapeutic Targets. Curr Neuropharmacol
811 *15*. 10.2174/1570159x14666160509123229.

812 2. Hayden, E., Holliday, H., Lehmann, R., Khan, A., Tsoli, M., Rayner, B.S., and
813 Ziegler, D.S. (2021). Therapeutic targets in diffuse midline gliomas—an emerging
814 landscape. Cancers (Basel) *13*. 10.3390/cancers13246251.

815 3. Ostrom, Q.T., Gittleman, H., Fulop, J., Liu, M., Blanda, R., Kromer, C., Wolinsky, Y.,
816 Kruchko, C., and Barnholtz-Sloan, J.S. (2015). CBTRUS statistical Report: primary
817 brain and central nervous system tumors diagnosed in the United States in 2008-2012.
818 Neuro Oncol *17*. 10.1093/neuonc/nov189.

819 4. Srikanthan, D., Taccone, M.S., Van Ommeren, R., Ishida, J., Krumholtz, S.L., and
820 Rutka, J.T. (2021). Diffuse intrinsic pontine glioma: current insights and future
821 directions. Chin Neurosurg J *7*. 10.1186/s41016-020-00218-w.

822 5. Castel, D., Philippe, C., Calmon, R., Le Dret, L., Truffaux, N., Boddaert, N., Pagès,
823 M., Taylor, K.R., Saulnier, P., Lacroix, L., et al. (2015). Histone H3F3A and
824 HIST1H3B K27M mutations define two subgroups of diffuse intrinsic pontine gliomas
825 with different prognosis and phenotypes. Acta Neuropathol *130*. 10.1007/s00401-015-
826 1478-0.

827 6. Fontebasso, A.M., Papillon-Cavanagh, S., Schwartzentruber, J., Nikbakht, H., Gerges,
828 N., Fiset, P.O., Bechet, D., Faury, D., De Jay, N., Ramkissoon, L.A., et al. (2014).
829 Recurrent somatic mutations in ACVR1 in pediatric midline high-grade astrocytoma.
830 Nat Genet *46*. 10.1038/ng.2950.

831 7. Schwartzentruber, J., Korshunov, A., Liu, X.Y., Jones, D.T.W., Pfaff, E., Jacob, K.,
832 Sturm, D., Fontebasso, A.M., Quang, D.A.K., Tönjes, M., et al. (2012). Erratum:
833 Driver mutations in histone H3.3 and chromatin remodelling genes in paediatric
834 glioblastoma (Nature (2012) 482 (226-231)). Nature *484*. 10.1038/nature11026.

835 8. Wu, G., Broniscer, A., McEachron, T.A., Lu, C., Paugh, B.S., Becksfort, J., Qu, C.,
836 Ding, L., Huether, R., Parker, M., et al. (2012). Somatic histone H3 alterations in
837 pediatric diffuse intrinsic pontine gliomas and non-brainstem glioblastomas. Nat Genet
838 *44*. 10.1038/ng.1102.

839 9. Bender, S., Tang, Y., Lindroth, A.M., Hovestadt, V., Jones, D.T.W., Kool, M.,
840 Zapatka, M., Northcott, P.A., Sturm, D., Wang, W., et al. (2013). Reduced H3K27me3

841 and DNA Hypomethylation Are Major Drivers of Gene Expression in K27M Mutant
842 Pediatric High-Grade Gliomas. Cancer Cell *24*. 10.1016/j.ccr.2013.10.006.

843 10. Chan, K.M., Fang, D., Gan, H., Hashizume, R., Yu, C., Schroeder, M., Gupta, N.,
844 Mueller, S., David James, C., Jenkins, R., et al. (2013). The histone H3.3K27M
845 mutation in pediatric glioma reprograms H3K27 methylation and gene expression.
846 Genes Dev *27*. 10.1101/gad.217778.113.

847 11. Lewis, P.W., Müller, M.M., Koletsky, M.S., Cordero, F., Lin, S., Banaszynski, L.A.,
848 Garcia, B.A., Muir, T.W., Becher, O.J., and Allis, C.D. (2013). Inhibition of PRC2
849 activity by a gain-of-function H3 mutation found in pediatric glioblastoma. Science
850 (1979) *340*. 10.1126/science.1232245.

851 12. Krug, B., De Jay, N., Harutyunyan, A.S., Deshmukh, S., Marchione, D.M.,
852 Guilhamon, P., Bertrand, K.C., Mikael, L.G., McConechy, M.K., Chen, C.C.L., et al.
853 (2019). Pervasive H3K27 Acetylation Leads to ERV Expression and a Therapeutic
854 Vulnerability in H3K27M Gliomas. Cancer Cell *35*. 10.1016/j.ccell.2019.04.004.

855 13. Piunti, A., Hashizume, R., Morgan, M.A., Bartom, E.T., Horbinski, C.M., Marshall,
856 S.A., Rendleman, E.J., Ma, Q., Takahashi, Y.H., Woodfin, A.R., et al. (2017).
857 Therapeutic targeting of polycomb and BET bromodomain proteins in diffuse intrinsic
858 pontine gliomas. Nat Med *23*. 10.1038/nm.4296.

859 14. Harpaz, N., Mittelman, T., Beresh, O., Griess, O., Furth, N., Salame, T.M., Oren, R.,
860 Fellus-Alyagor, L., Harmelin, A., Alexandrescu, S., et al. (2022). Single-cell
861 epigenetic analysis reveals principles of chromatin states in H3.3-K27M gliomas. Mol
862 Cell *82*, 2696-2713.e9. 10.1016/j.molcel.2022.05.023.

863 15. Filbin, M., and Monje, M. (2019). Developmental origins and emerging therapeutic
864 opportunities for childhood cancer. Nat Med *25*. 10.1038/s41591-019-0383-9.

865 16. Furth, N., Algranati, D., Dassa, B., Beresh, O., Fedyuk, V., Morris, N., Kasper, L.H.,
866 Jones, D., Monje, M., Baker, S.J., et al. (2022). H3-K27M-mutant nucleosomes
867 interact with MLL1 to shape the glioma epigenetic landscape. Cell Rep *39*.
868 10.1016/j.celrep.2022.110836.

869 17. Grasso, C.S., Tang, Y., Truffaux, N., Berlow, N.E., Liu, L., Debily, M.A., Quist, M.J.,
870 Davis, L.E., Huang, E.C., Woo, P.J., et al. (2015). Functionally defined therapeutic
871 targets in diffuse intrinsic pontine glioma. Nat Med *21*. 10.1038/nm.3855.

872 18. Yin, D., Ong, J.M., Hu, J., Desmond, J.C., Kawamata, N., Konda, B.M., Black, K.L.,
873 and Koeffler, H.P. (2007). Suberoylanilide hydroxamic acid, a histone deacetylase

874 inhibitor: Effects on gene expression and growth of glioma cells in vitro and in vivo.
875 Clinical Cancer Research *13*. 10.1158/1078-0432.CCR-06-1261.

876 19. Su, J.M., Kilburn, L.B., Mansur, D.B., Krailo, M., Buxton, A., Adekunle, A., Gajjar,
877 A., Adamson, P.C., Weigel, B., Fox, E., et al. (2022). Phase I/II trial of vorinostat and
878 radiation and maintenance vorinostat in children with diffuse intrinsic pontine glioma:
879 A Children's Oncology Group report. Neuro Oncol *24*. 10.1093/neuonc/noab188.

880 20. Chen, H., Liu, H., and Qing, G. (2018). Targeting oncogenic Myc as a strategy for
881 cancer treatment. Signal Transduct Target Ther *3*. 10.1038/s41392-018-0008-7.

882 21. Buczkowicz, P., Hoeman, C., Rakopoulos, P., Pajovic, S., Letourneau, L., Dzamba,
883 M., Morrison, A., Lewis, P., Bouffet, E., Bartels, U., et al. (2014). Genomic analysis
884 of diffuse intrinsic pontine gliomas identifies three molecular subgroups and recurrent
885 activating ACVR1 mutations. Nat Genet *46*. 10.1038/ng.2936.

886 22. Mackay, A., Burford, A., Carvalho, D., Izquierdo, E., Fazal-Salom, J., Taylor, K.R.,
887 Bjerke, L., Clarke, M., Vinci, M., Nandhabalan, M., et al. (2017). Integrated
888 Molecular Meta-Analysis of 1,000 Pediatric High-Grade and Diffuse Intrinsic Pontine
889 Glioma. Cancer Cell *32*. 10.1016/j.ccell.2017.08.017.

890 23. Pajovic, S., Siddaway, R., Bridge, T., Sheth, J., Rakopoulos, P., Kim, B., Ryall, S.,
891 Agnihotri, S., Phillips, L., Yu, M., et al. (2020). Epigenetic activation of a RAS/MYC
892 axis in H3.3K27M-driven cancer. Nat Commun *11*. 10.1038/s41467-020-19972-7.

893 24. Dubois, F.P.B., Shapira, O., Greenwald, N.F., Zack, T., Wala, J., Tsai, J.W., Crane,
894 A., Baguette, A., Hadjadj, D., Harutyunyan, A.S., et al. (2022). Structural variants
895 shape driver combinations and outcomes in pediatric high-grade glioma. Nat Cancer *3*,
896 994–1011. 10.1038/s43018-022-00403-z.

897 25. Wang, C., Zhang, J., Yin, J., Gan, Y., Xu, S., Gu, Y., and Huang, W. (2021).
898 Alternative approaches to target Myc for cancer treatment. Signal Transduct Target
899 Ther *6*. 10.1038/s41392-021-00500-y.

900 26. Dubiella, C., Pinch, B.J., Koikawa, K., Zaidman, D., Poon, E., Manz, T.D., Nabet, B.,
901 He, S., Resnick, E., Rogel, A., et al. (2021). Sulfopin is a covalent inhibitor of Pin1
902 that blocks Myc-driven tumors in vivo. Nat Chem Biol *17*. 10.1038/s41589-021-
903 00786-7.

904 27. Farrell, A.S., Pelz, C., Wang, X., Daniel, C.J., Wang, Z., Su, Y., Janghorban, M.,
905 Zhang, X., Morgan, C., Impey, S., et al. (2013). Pin1 Regulates the Dynamics of c-
906 Myc DNA Binding To Facilitate Target Gene Regulation and Oncogenesis. Mol Cell
907 Biol *33*. 10.1128/mcb.01455-12.

908 28. D'Artista, L., Bisso, A., Piontini, A., Doni, M., Verrecchia, A., Kress, T.R., Morelli,
909 M.J., Del Sal, G., Amati, B., and Campaner, S. (2016). Pin1 is required for sustained B
910 cell proliferation upon oncogenic activation of Myc. Oncotarget *7*.
911 10.18632/oncotarget.7846.

912 29. Hölzel, M., Rohrmoser, M., Schlee, M., Grimm, T., Harasim, T., Malamoussi, A.,
913 Gruber-Eber, A., Kremmer, E., Hiddemann, W., Bornkamm, G.W., et al. (2005).
914 Mammalian WDR12 is a novel member of the Pes1-Bop1 complex and is required for
915 ribosome biogenesis and cell proliferation. Journal of Cell Biology *170*.
916 10.1083/jcb.200501141.

917 30. Teng, S.C., Chen, Y.Y., Su, Y.N., Chou, P.C., Chiang, Y.C., Tseng, S.F., and Wu, K.J.
918 (2004). Direct Activation of HSP90A Transcription by c-Myc Contributes to c-Myc-
919 induced Transformation. Journal of Biological Chemistry *279*.
920 10.1074/jbc.M308842200.

921 31. Skene, P.J., and Henikoff, S. (2017). An efficient targeted nuclease strategy for high-
922 resolution mapping of DNA binding sites. Elife *6*. 10.7554/eLife.21856.

923 32. Ferrari, K.J., Scelfo, A., Jammula, S.G., Cuomo, A., Barozzi, I., Stützer, A., Fischle,
924 W., Bonaldi, T., and Pasini, D. (2014). Polycomb-Dependent H3K27me1 and
925 H3K27me2 Regulate Active Transcription and Enhancer Fidelity. Mol Cell *53*.
926 10.1016/j.molcel.2013.10.030.

927 33. Mohammad, F., Weissmann, S., Leblanc, B., Pandey, D.P., Højfeldt, J.W., Comet, I.,
928 Zheng, C., Johansen, J.V., Rapin, N., Porse, B.T., et al. (2017). EZH2 is a potential
929 therapeutic target for H3K27M-mutant pediatric gliomas. Nat Med *23*.
930 10.1038/nm.4293.

931 34. Jain, S.U., Rashoff, A.Q., Krabbenhoft, S.D., Hoelper, D., Do, T.J., Gibson, T.J.,
932 Lundgren, S.M., Bondra, E.R., Deshmukh, S., Harutyunyan, A.S., et al. (2020). H3
933 K27M and EZHIP Impede H3K27-Methylation Spreading by Inhibiting Allosterically
934 Stimulated PRC2. Mol Cell *80*. 10.1016/j.molcel.2020.09.028.

935 35. Berlow, N.E., Svalina, M.N., Quist, M.J., Settelmeyer, T.P., Zherebitskiy, V., Kogiso,
936 M., Qi, L., Du, Y., Hawkins, C.E., Hulleman, E., et al. (2018). IL-13 receptors as
937 possible therapeutic targets in diffuse intrinsic pontine glioma. PLoS One *13*.
938 10.1371/journal.pone.0193565.

939 36. Yeh, E.S., and Means, A.R. (2007). PIN1, the cell cycle and cancer. Nat Rev Cancer *7*.
940 10.1038/nrc2107.

941 37. Pinch, B.J., Doctor, Z.M., Nabet, B., Browne, C.M., Seo, H.S., Mohardt, M.L.,
942 Kozono, S., Lian, X., Manz, T.D., Chun, Y., et al. (2020). Identification of a potent
943 and selective covalent Pin1 inhibitor. Nat Chem Biol *16*. 10.1038/s41589-020-0550-9.

944 38. Lin, G.L., Wilson, K.M., Ceribelli, M., Stanton, B.Z., Woo, P.J., Kreimer, S., Qin,
945 E.Y., Zhang, X., Lennon, J., Nagaraja, S., et al. (2019). Therapeutic strategies for
946 diffuse midline glioma from high-throughput combination drug screening. Sci Transl
947 Med *11*. 10.1126/scitranslmed.aaw0064.

948 39. Harutyunyan, A.S., Krug, B., Chen, H., Papillon-Cavanagh, S., Zeinieh, M., De Jay,
949 N., Deshmukh, S., Chen, C.C.L., Belle, J., Mikael, L.G., et al. (2019). H3K27M
950 induces defective chromatin spread of PRC2-mediated repressive H3K27me2/me3 and
951 is essential for glioma tumorigenesis. Nat Commun *10*. 10.1038/s41467-019-09140-x.

952 40. Schuettengruber, B., Bourbon, H.M., Di Croce, L., and Cavalli, G. (2017). Genome
953 Regulation by Polycomb and Trithorax: 70 Years and Counting. Cell *171*.
954 10.1016/j.cell.2017.08.002.

955 41. Stafford, J.M., Lee, C.H., Voigt, P., Descostes, N., Saldana-Meyer, R., Yu, J.R.,
956 Leroy, G., Oksuz, O., Chapman, J.R., Suarez, F., et al. (2018). Multiple modes of
957 PRC2 inhibition elicit global chromatin alterations in H3K27M pediatric glioma. Sci
958 Adv *4*. 10.1126/sciadv.aau5935.

959 42. Jain, S.U., Do, T.J., Lund, P.J., Rashoff, A.Q., Diehl, K.L., Cieslik, M., Bajic, A.,
960 Juretic, N., Deshmukh, S., Venneti, S., et al. (2019). PFA ependymoma-associated
961 protein EZHIP inhibits PRC2 activity through a H3 K27M-like mechanism. Nat
962 Commun *10*. 10.1038/s41467-019-09981-6.

963 43. Agger, K., Cloos, P.A.C., Christensen, J., Pasini, D., Rose, S., Rappsilber, J., Issaeva,
964 I., Canaani, E., Salcini, A.E., and Helin, K. (2007). UTX and JMJD3 are histone
965 H3K27 demethylases involved in HOX gene regulation and development. Nature *449*.
966 10.1038/nature06145.

967 44. Hashizume, R., Andor, N., Ihara, Y., Lerner, R., Gan, H., Chen, X., Fang, D., Huang,
968 X., Tom, M.W., Ngo, V., et al. (2014). Pharmacologic inhibition of histone
969 demethylation as a therapy for pediatric brainstem glioma. Nat Med *20*.
970 10.1038/nm.3716.

971 45. Yadav, B., Wennerberg, K., Aittokallio, T., and Tang, J. (2015). Searching for Drug
972 Synergy in Complex Dose-Response Landscapes Using an Interaction Potency Model.
973 Comput Struct Biotechnol J *13*. 10.1016/j.csbj.2015.09.001.

974 46. BLISS, C.I. (1939). THE TOXICITY OF POISONS APPLIED JOINTLY. Annals of
975 Applied Biology *26*. 10.1111/j.1744-7348.1939.tb06990.x.

976 47. Nagaraja, S., Quezada, M.A., Gillespie, S.M., Arzt, M., Lennon, J.J., Woo, P.J.,
977 Hovestadt, V., Kambhampati, M., Filbin, M.G., Suva, M.L., et al. (2019). Histone
978 Variant and Cell Context Determine H3K27M Reprogramming of the Enhancer
979 Landscape and Oncogenic State. Mol Cell *76*. 10.1016/j.molcel.2019.08.030.

980 48. Jessa, S., Mohammadnia, A., Harutyunyan, A.S., Hulswit, M., Varadharajan, S.,
981 Lakkis, H., Kabir, N., Bashardanesh, Z., Hébert, S., Faury, D., et al. (2022). K27M in
982 canonical and noncanonical H3 variants occurs in distinct oligodendroglial cell
983 lineages in brain midline gliomas. Nat Genet *54*. 10.1038/s41588-022-01205-w.

984 49. Annovazzi, L., Mellai, M., Caldera, V., Valente, G., Tessitore, L., and Schiffer, D.
985 (2009). mTOR, S6 and AKT expression in relation to proliferation and
986 apoptosis/autophagy in glioma. Anticancer Res *29*.

987 50. Ma, S., Pang, C., Song, L., Guo, F., and Sun, H. (2015). Activating transcription factor
988 3 is overexpressed in human glioma and its knockdown in glioblastoma cells causes
989 growth inhibition both in vitro and in vivo. Int J Mol Med *35*.
990 10.3892/ijmm.2015.2173.

991 51. Xue, H., Zhang, J., Guo, X., Wang, J., Li, J., Gao, X., Guo, X., Li, T., Xu, S., Zhang,
992 P., et al. (2016). CREBRF is a potent tumor suppressor of glioblastoma by blocking
993 hypoxia-induced autophagy via the CREB3/ATG5 pathway. Int J Oncol *49*.
994 10.3892/ijo.2016.3576.

995 52. Tang, P., Steck, P.A., and Yung, W.K.A. (1997). The autocrine loop of TGF-α/EGFR
996 and brain tumors. J Neurooncol *35*. 10.1023/A:1005824802617.

997 53. Abdouh, M., Facchino, S., Chatoo, W., Balasingam, V., Ferreira, J., and Bernier, G.
998 (2009). BMI1 sustains human glioblastoma multiforme stem cell renewal. Journal of
999 Neuroscience *29*. 10.1523/JNEUROSCI.0968-09.2009.

1000 54. Zhang, H., Kong, Q., Wang, J., Jiang, Y., and Hua, H. (2020). Complex roles of
1001 cAMP–PKA–CREB signaling in cancer. Exp Hematol Oncol *9*. 10.1186/s40164-020-
1002 00191-1.

1003 55. West, A.J., Tsui, V., Stylli, S.S., Nguyen, H.P.T., Morokoff, A.P., Kaye, A.H., and
1004 Luwor, R.B. (2018). The role of interleukin-6-STAT3 signalling in glioblastoma.
1005 Oncol Lett *16*. 10.3892/ol.2018.9227.

1006 56. Kennedy, B.K., and Lamming, D.W. (2016). The Mechanistic Target of Rapamycin:
1007 The Grand ConducTOR of Metabolism and Aging. Cell Metab *23*.
1008 10.1016/j.cmet.2016.05.009.

1009 57. Shamloo, B., and Usluer, S. (2019). P21 in cancer research. Cancers (Basel) *11*.
1010 10.3390/cancers11081178.

1011 58. Tahmasebi, S., Alain, T., Rajasekhar, V.K., Zhang, J.P., Prager-Khoutorsky, M.,
1012 Khoutorsky, A., Dogan, Y., Gkogkas, C.G., Petroulakis, E., Sylvestre, A., et al.
1013 (2014). Multifaceted regulation of somatic cell reprogramming by mRNA translational
1014 control. Cell Stem Cell *14*. 10.1016/j.stem.2014.02.005.

1015 59. Cui, D., Qu, R., Liu, D., Xiong, X., Liang, T., and Zhao, Y. (2021). The Cross Talk
1016 Between p53 and mTOR Pathways in Response to Physiological and Genotoxic
1017 Stresses. Front Cell Dev Biol *9*. 10.3389/fcell.2021.775507.

1018 60. Minucci, S., and Pelicci, P.G. (2006). Histone deacetylase inhibitors and the promise
1019 of epigenetic (and more) treatments for cancer. Nat Rev Cancer *6*. 10.1038/nrc1779.

1020 61. Poole, C.J., and van Riggelen, J. (2017). MYC—master regulator of the cancer
1021 epigenome and transcriptome. Genes (Basel) *8*. 10.3390/genes8050142.

1022 62. Kanai, Y. (2022). Amino acid transporter LAT1 (SLC7A5) as a molecular target for
1023 cancer diagnosis and therapeutics. Pharmacol Ther *230*.
1024 10.1016/j.pharmthera.2021.107964.

1025 63. Lee, D.W., Ramakrishnan, D., Valenta, J., Parney, I.F., Bayless, K.J., and Sitcheran,
1026 R. (2013). The NF-κB RelB Protein Is an Oncogenic Driver of Mesenchymal Glioma.
1027 PLoS One *8*. 10.1371/journal.pone.0057489.

1028 64. Feng, Y., Lei, X., Zhang, L., Wan, H., Pan, H., Wu, J., Zou, M., Zhu, L., and Mi, Y.
1029 (2021). COPB2: a transport protein with multifaceted roles in cancer development and
1030 progression. Clinical and Translational Oncology *23*. 10.1007/s12094-021-02630-9.

1031 65. Zhou, D., Tang, W., Su, G., Cai, M., An, H.X., and Zhang, Y. (2017). PCDH18 is
1032 frequently inactivated by promoter methylation in colorectal cancer. Sci Rep *7*.
1033 10.1038/s41598-017-03133-w.

1034 66. Fernández-Medarde, A., and Santos, E. (2011). Ras in cancer and developmental
1035 diseases. Genes Cancer *2*. 10.1177/1947601911411084.

1036 67. Braicu, C., Buse, M., Busuioc, C., Drula, R., Gulei, D., Raduly, L., Rusu, A., Irimie,
1037 A., Atanasov, A.G., Slaby, O., et al. (2019). A comprehensive review on MAPK: A
1038 promising therapeutic target in cancer. Cancers (Basel) *11*. 10.3390/cancers11101618.

1039 68. Rascio, F., Spadaccino, F., Rocchetti, M.T., Castellano, G., Stallone, G., Netti, G.S.,
1040 and Ranieri, E. (2021). The pathogenic role of PI3K/AKT pathway in cancer onset and
1041 drug resistance: an updated review. Cancers (Basel) *13*. 10.3390/cancers13163949.

1042 69. Peng, Y., Wang, Y., Zhou, C., Mei, W., and Zeng, C. (2022). PI3K/Akt/mTOR
1043 Pathway and Its Role in Cancer Therapeutics: Are We Making Headway? Front Oncol
1044 *12*. 10.3389/fonc.2022.819128.

1045 70. Mure, H., Matsuzaki, K., Kitazato, K.T., Mizobuchi, Y., Kuwayama, K., Kageji, T.,
1046 and Nagahiro, S. (2010). Akt2 and Akt3 play a pivotal role in malignant gliomas.
1047 Neuro Oncol *12*. 10.1093/neuonc/nop026.

1048 71. Ding, Z., Kloss, J.M., Tuncali, S., Tran, N.L., and Loftus, J.C. (2020). TROY signals
1049 through JAK1-STAT3 to promote glioblastoma cell migration and resistance.
1050 Neoplasia (United States) *22*. 10.1016/j.neo.2020.06.005.

1051 72. Tu, Y., Zhong, Y., Fu, J., Cao, Y., Fu, G., Tian, X., and Wang, B. (2011). Activation
1052 of JAK/STAT signal pathway predicts poor prognosis of patients with gliomas.
1053 Medical Oncology *28*. 10.1007/s12032-010-9435-1.

1054 73. Raychaudhuri, B., Han, Y., Lu, T., and Vogelbaum, M.A. (2007). Aberrant
1055 constitutive activation of nuclear factor κB in glioblastoma multiforme drives invasive
1056 phenotype. J Neurooncol *85*. 10.1007/s11060-007-9390-7.

1057 74. Bar-Peled, L., Chantranupong, L., Cherniack, A.D., Chen, W.W., Ottina, K.A.,
1058 Grabiner, B.C., Spear, E.D., Carter, S.L., Meyerson, M., and Sabatini, D.M. (2013). A
1059 tumor suppressor complex with GAP activity for the Rag GTPases that signal amino
1060 acid sufficiency to mTORC1. Science (1979) *340*. 10.1126/science.1232044.

1061 75. Cai, W., Wei, Y., Jarnik, M., Reich, J., and Lilly, M.A. (2016). The GATOR2
1062 Component Wdr24 Regulates TORC1 Activity and Lysosome Function. PLoS Genet
1063 *12*. 10.1371/journal.pgen.1006036.

1064 76. Langenkamp, E., Zhang, L., Lugano, R., Huang, H., Elhassan, T.E.A., Georganaki,
1065 M., Bazzar, W., Lööf, J., Trendelenburg, G., Essand, M., et al. (2015). Elevated
1066 expression of the C-Type Lectin CD93 in the glioblastoma vasculature regulates
1067 cytoskeletal rearrangements that enhance vessel function and reduce host survival.
1068 Cancer Res *75*. 10.1158/0008-5472.CAN-14-3636.

1069 77. Sharma, S. V., Lee, D.Y., Li, B., Quinlan, M.P., Takahashi, F., Maheswaran, S.,
1070 McDermott, U., Azizian, N., Zou, L., Fischbach, M.A., et al. (2010). A Chromatin-
1071 Mediated Reversible Drug-Tolerant State in Cancer Cell Subpopulations. Cell *141*.
1072 10.1016/j.cell.2010.02.027.

1073 78. Knoechel, B., Roderick, J.E., Williamson, K.E., Zhu, J., Lohr, J.G., Cotton, M.J.,
1074 Gillespie, S.M., Fernandez, D., Ku, M., Wang, H., et al. (2014). An epigenetic
1075 mechanism of resistance to targeted therapy in T cell acute lymphoblastic leukemia.
1076 Nat Genet *46*. 10.1038/ng.2913.

1077 79. Nagaraja, S., Vitanza, N.A., Woo, P.J., Taylor, K.R., Liu, F., Zhang, L., Li, M., Meng,
1078 W., Ponnuswami, A., Sun, W., et al. (2017). Transcriptional Dependencies in Diffuse
1079 Intrinsic Pontine Glioma. Cancer Cell *31*. 10.1016/j.ccell.2017.03.011.

1080 80. Cooney, T., Onar-Thomas, A., Huang, J., Lulla, R., Fangusaro, J., Kramer, K., Baxter,
1081 P., Fouladi, M., Dunkel, I.J., Warren, K.E., et al. (2018). DIPG-22. A PHASE 1
1082 TRIAL OF THE HISTONE DEACETYLASE INHIBITOR PANOBINOSTAT IN
1083 PEDIATRIC PATIENTS WITH RECURRENT OR REFRACTORY DIFFUSE
1084 INTRINSIC PONTINE GLIOMA: A PEDIATRIC BRAIN TUMOR CONSORTIUM
1085 (PBTC) STUDY. Neuro Oncol *20*. 10.1093/neuonc/noy059.115.

1086 81. Hennika, T., Hu, G., Olaciregui, N.G., Barton, K.L., Ehteda, A., Chitranjan, A.,
1087 Chang, C., Gifford, A.J., Tsoli, M., Ziegler, D.S., et al. (2017). Pre-clinical study of
1088 panobinostat in xenograft and genetically engineered murine diffuse intrinsic pontine
1089 glioma models. PLoS One *12*. 10.1371/journal.pone.0169485.

1090 82. Leszczynska, K.B., Jayaprakash, C., Kaminska, B., and Mieczkowski, J. (2021).
1091 Emerging Advances in Combinatorial Treatments of Epigenetically Altered Pediatric
1092 High-Grade H3K27M Gliomas. Front Genet *12*. 10.3389/fgene.2021.742561.

1093 83. Oster, S.K., Ho, C.S.W., Soucie, E.L., and Penn, L.Z. (2002). The myc oncogene:
1094 Marvelously complex. Adv Cancer Res *84*. 10.1016/S0065-230X(02)84004-0.

1095 84. Pelengaris, S., Khan, M., and Evan, G. (2002). c-MYC: More than just a matter of life
1096 and death. Nat Rev Cancer *2*. 10.1038/nrc904.

1097 85. Akhavan, D., Cloughesy, T.F., and Mischel, P.S. (2010). mTOR signaling in
1098 glioblastoma: Lessons learned from bench to bedside. Neuro Oncol *12*.
1099 10.1093/neuonc/noq052.

1100 86. Warren, K.E., Killian, K., Suuriniemi, M., Wang, Y., Quezado, M., and Meltzer, P.S.
1101 (2012). Genomic aberrations in pediatric diffuse intrinsic pontine gliomas. Neuro
1102 Oncol *14*. 10.1093/neuonc/nor190.

1103 87. Panditharatna, E., Yaeger, K., Kilburn, L.B., Packer, R.J., and Nazarian, J. (2015).
1104 Clinicopathology of diffuse intrinsic pontine glioma and its redefined genomic and
1105 epigenomic landscape. Cancer Genet *208*. 10.1016/j.cancergen.2015.04.008.

1106 88. Zarghooni, M., Bartels, U., Lee, E., Buczkowicz, P., Morrison, A., Huang, A.,
1107 Bouffet, E., and Hawkins, C. (2010). Whole-genome profiling of pediatric diffuse
1108 intrinsic pontine gliomas highlights platelet-derived growth factor receptor α and poly
1109 (ADP-ribose) polymerase as potential therapeutic targets. Journal of Clinical
1110 Oncology *28*. 10.1200/JCO.2009.25.5463.

1111 89. Tsoli, M., Liu, J., Franshaw, L., Shen, H., Cheng, C., Jung, M.S., Joshi, S., Ehteda, A.,
1112 Khan, A., Montero-Carcabosso, A., et al. (2018). Dual targeting of mitochondrial
1113 function and mTOR pathway as a therapeutic strategy for diffuse intrinsic pontine
1114 glioma. Oncotarget *9*. 10.18632/oncotarget.24045.

1115 90. Guertin, D.A., and Sabatini, D.M. (2009). The pharmacology of mTOR inhibition. Sci
1116 Signal *2*. 10.1126/scisignal.267pe24.

1117 91. Zoncu, R., Efeyan, A., and Sabatini, D.M. (2011). MTOR: From growth signal
1118 integration to cancer, diabetes and ageing. Nat Rev Mol Cell Biol *12*.
1119 10.1038/nrm3025.

1120 92. Schmidt, E. V., Ravitz, M.J., Chen, L., and Lynch, M. (2009). Growth controls
1121 connect: Interactions between c-myc and the tuberous sclerosis complex-mTOR
1122 pathway. Cell Cycle *8*. 10.4161/cc.8.9.8215.

1123 93. Sodi, V.L., Khaku, S., Krutilina, R., Schwab, L.P., Vocadlo, D.J., Seagroves, T.N.,
1124 and Reginato, M.J. (2015). MTOR/MYCAxis regulates O-GlcNAc transferase
1125 expression and O-GlcN acylation in breast cancer. Molecular Cancer Research *13*.
1126 10.1158/1541-7786.MCR-14-0536.

1127 94. Kuo, Y., Huang, H., Cai, T., and Wang, T. (2015). Target of rapamycin complex 2
1128 regulates cell growth via Myc in drosophila. Sci Rep *5*. 10.1038/srep10339.

1129 95. Miyahara, H., Yadavilli, S., Natsumeda, M., Rubens, J.A., Rodgers, L., Kambhampati,
1130 M., Taylor, I.C., Kaur, H., Asnaghi, L., Eberhart, C.G., et al. (2017). The dual mTOR
1131 kinase inhibitor TAK228 inhibits tumorigenicity and enhances radiosensitization in
1132 diffuse intrinsic pontine glioma. Cancer Lett *400*. 10.1016/j.canlet.2017.04.019.

1133 96. Flannery, P.C., DeSisto, J.A., Amani, V., Venkataraman, S., Lemma, R.T., Prince,
1134 E.W., Donson, A., Moroze, E.E., Hoffman, L., Levy, J.M.M., et al. (2018). Preclinical
1135 analysis of MTOR complex 1/2 inhibition in diffuse intrinsic pontine glioma. Oncol
1136 Rep *39*. 10.3892/or.2017.6122.

1137 97. Schlee, M., Schuhmacher, M., Hölzel, M., Laux, G., and Bornkamm, G.W. (2007). c-
1138 MYC Impairs Immunogenicity of Human B Cells. Adv Cancer Res *97*.
1139 10.1016/S0065-230X(06)97007-9.

1140 98. Jones, P.A., Ohtani, H., Chakravarthy, A., and De Carvalho, D.D. (2019). Epigenetic
1141 therapy in immune-oncology. Nat Rev Cancer *19*. 10.1038/s41568-019-0109-9.

1142 99. See, Y.X., Chen, K., and Fullwood, M.J. (2022). MYC overexpression leads to
1143 increased chromatin interactions at super-enhancers and MYC binding sites. Genome
1144 Res *32*. 10.1101/gr.276313.121.

1145 100. Jaitin, D.A., Kenigsberg, E., Keren-Shaul, H., Elefant, N., Paul, F., Zaretsky, I.,
1146 Mildner, A., Cohen, N., Jung, S., Tanay, A., et al. (2014). Massively parallel single-
1147 cell RNA-seq for marker-free decomposition of tissues into cell types. Science (1979)
1148 *343*. 10.1126/science.1247651.

1149 101. Keren-Shaul, H., Kenigsberg, E., Jaitin, D.A., David, E., Paul, F., Tanay, A., and
1150 Amit, I. (2019). MARS-seq2.0: an experimental and analytical pipeline for indexed
1151 sorting combined with single-cell RNA sequencing. Nat Protoc *14*. 10.1038/s41596-
1152 019-0164-4.

1153 102. Meers, M.P., Bryson, T.D., Henikoff, J.G., and Henikoff, S. (2019). Improved
1154 cut&run chromatin profiling tools. Elife *8*. 10.7554/ELIFE.46314.

1155 103. Blecher-Gonen, R., Barnett-Itzhaki, Z., Jaitin, D., Amann-Zalcenstein, D., Lara-
1156 Astiaso, D., and Amit, I. (2013). High-throughput chromatin immunoprecipitation for
1157 genome-wide mapping of in vivo protein-DNA interactions and epigenomic states.
1158 Nat Protoc *8*. 10.1038/nprot.2013.023.

1159 104. Venkatesh, H.S., Morishita, W., Geraghty, A.C., Silverbush, D., Gillespie, S.M., Arzt,
1160 M., Tam, L.T., Espenel, C., Ponnuswami, A., Ni, L., et al. (2019). Electrical and
1161 synaptic integration of glioma into neural circuits. Nature *573*. 10.1038/s41586-019-
1162 1563-y.

1163 105. Martin, M. (2011). Cutadapt removes adapter sequences from high-throughput
1164 sequencing reads. EMBnet J *17*. 10.14806/ej.17.1.200.

1165 106. Langmead, B., and Salzberg, S.L. (2012). Fast gapped-read alignment with Bowtie 2.
1166 Nat Methods *9*. 10.1038/nmeth.1923.

1167 107. Yu, G., Wang, L.G., and He, Q.Y. (2015). ChIP seeker: An R/Bioconductor package
1168 for ChIP peak annotation, comparison and visualization. Bioinformatics *31*.
1169 10.1093/bioinformatics/btv145.

1170 108. Shen, L., Shao, N., Liu, X., and Nestler, E. (2014). Ngs.plot: Quick mining and
1171 visualization of next-generation sequencing data by integrating genomic databases.
1172 BMC Genomics *15*. 10.1186/1471-2164-15-284.

1173 109. McLean, C.Y., Bristor, D., Hiller, M., Clarke, S.L., Schaar, B.T., Lowe, C.B., Wenger,
1174 A.M., and Bejerano, G. (2010). GREAT improves functional interpretation of cis-
1175 regulatory regions. Nat Biotechnol *28*. 10.1038/nbt.1630.

1176 110. Ramírez, F., Ryan, D.P., Grüning, B., Bhardwaj, V., Kilpert, F., Richter, A.S., Heyne,
1177 S., Dündar, F., and Manke, T. (2016). deepTools2: a next generation web server for
1178 deep-sequencing data analysis. Nucleic Acids Res *44*. 10.1093/NAR/GKW257.

1179 111. Quinlan, A.R., and Hall, I.M. (2010). BEDTools: A flexible suite of utilities for
1180 comparing genomic features. Bioinformatics *26*. 10.1093/bioinformatics/btq033.

1181 112. Fishilevich, S., Nudel, R., Rappaport, N., Hadar, R., Plaschkes, I., Stein, T.I., Rosen,
1182 N., Kohn, A., Twik, M., Safran, M., et al. (2017). GeneHancer: Genome-wide
1183 integration of enhancers and target genes in GeneCards. Database *2017*.
1184 10.1093/database/bax028.

1185 113. Kohen, R., Barlev, J., Hornung, G., Stelzer, G., Feldmesser, E., Kogan, K., Safran, M.,
1186 and Leshkowitz, D. (2019). UTAP: User-friendly Transcriptome Analysis Pipeline.
1187 BMC Bioinformatics *20*. 10.1186/s12859-019-2728-2.

1188 114. Dobin, A., Davis, C.A., Schlesinger, F., Drenkow, J., Zaleski, C., Jha, S., Batut, P.,
1189 Chaisson, M., and Gingeras, T.R. (2013). STAR: Ultrafast universal RNA-seq aligner.
1190 Bioinformatics *29*. 10.1093/bioinformatics/bts635.

1191 115. Anders, S., Pyl, P.T., and Huber, W. (2015). HTSeq-A Python framework to work
1192 with high-throughput sequencing data. Bioinformatics *31*.
1193 10.1093/bioinformatics/btu638.

1194 116. Love, M.I., Huber, W., and Anders, S. (2014). Moderated estimation of fold change
1195 and dispersion for RNA-seq data with DESeq2. Genome Biol *15*. 10.1186/s13059-
1196 014-0550-8.

1197 117. Subramanian, A., Tamayo, P., Mootha, V.K., Mukherjee, S., Ebert, B.L., Gillette,
1198 M.A., Paulovich, A., Pomeroy, S.L., Golub, T.R., Lander, E.S., et al. (2005). Gene set
1199 enrichment analysis: A knowledge-based approach for interpreting genome-wide
1200 expression profiles. Proc Natl Acad Sci U S A *102*. 10.1073/pnas.0506580102.

1201 118. Mootha, V.K., Lindgren, C.M., Eriksson, K.F., Subramanian, A., Sihag, S., Lehar, J.,
1202 Puigserver, P., Carlsson, E., Ridderstråle, M., Laurila, E., et al. (2003). PGC-1α-
1203 responsive genes involved in oxidative phosphorylation are coordinately
1204 downregulated in human diabetes. Nat Genet *34*. 10.1038/ng1180.

1205 119. Liberzon, A., Birger, C., Thorvaldsdóttir, H., Ghandi, M., Mesirov, J.P., and Tamayo,
1206 P. (2015). The Molecular Signatures Database Hallmark Gene Set Collection. Cell
1207 Syst *1*. 10.1016/j.cels.2015.12.004.

1208 120. Wiederschain, D., Chen, L., Johnson, B., Bettano, K., Jackson, D., Taraszka, J., Wang,
1209 Y.K., Jones, M.D., Morrissey, M., Deeds, J., et al. (2007). Contribution of Polycomb
1210 Homologues Bmi-1 and Mel-18 to Medulloblastoma Pathogenesis. Mol Cell Biol *27*.
1211 10.1128/mcb.02244-06.

1212 121. Van Staveren, W.C.G., Solís, D.W., Delys, L., Venet, D., Cappello, M., Andry, G.,
1213 Dumont, J.E., Libert, F., Detours, V., and Maenhaut, C. (2006). Gene expression in
1214 human thyrocytes and autonomous adenomas reveals suppression of negative
1215 feedbacks in tumorigenesis. Proc Natl Acad Sci U S A *103*.
1216 10.1073/pnas.0507354102.

1217 122. Wei, G., Twomey, D., Lamb, J., Schlis, K., Agarwal, J., Stam, R.W., Opferman, J.T.,
1218 Sallan, S.E., den Boer, M.L., Pieters, R., et al. (2006). Gene expression-based
1219 chemical genomics identifies rapamycin as a modulator of MCL1 and glucocorticoid
1220 resistance. Cancer Cell *10*. 10.1016/j.ccr.2006.09.006.

1221 123. Kuleshov, M. V., Jones, M.R., Rouillard, A.D., Fernandez, N.F., Duan, Q., Wang, Z.,
1222 Koplev, S., Jenkins, S.L., Jagodnik, K.M., Lachmann, A., et al. (2016). Enrichr: a
1223 comprehensive gene set enrichment analysis web server 2016 update. Nucleic Acids
1224 Res *44*. 10.1093/nar/gkw377.

1225 124. Keenan, A.B., Torre, D., Lachmann, A., Leong, A.K., Wojciechowicz, M.L., Utti, V.,
1226 Jagodnik, K.M., Kropiwnicki, E., Wang, Z., and Ma'ayan, A. (2019). ChEA3:
1227 transcription factor enrichment analysis by orthogonal omics integration. Nucleic
1228 Acids Res *47*. 10.1093/nar/gkz446.

1229 125. Dunham, I., Kundaje, A., Aldred, S.F., Collins, P.J., Davis, C.A., Doyle, F., Epstein,
1230 C.B., Frietze, S., Harrow, J., Kaul, R., et al. (2012). An integrated encyclopedia of
1231 DNA elements in the human genome. Nature *489*. 10.1038/nature11247.

1232 126. Raudvere, U., Kolberg, L., Kuzmin, I., Arak, T., Adler, P., Peterson, H., and Vilo, J.
1233 (2019). G:Profiler: A web server for functional enrichment analysis and conversions of
1234 gene lists (2019 update). Nucleic Acids Res *47*. 10.1093/nar/gkz369.

1235 127. Kanehisa, M. (2019). Toward understanding the origin and evolution of cellular
1236 organisms. Protein Science *28*. 10.1002/pro.3715.

1237 128. Kanehisa, M., and Goto, S. (2000). KEGG: Kyoto Encyclopedia of Genes and
1238 Genomes. Nucleic Acids Res *28*. 10.1093/nar/28.1.27.

129. Martens, M., Ammar, A., Riutta, A., Waagmeester, A., Slenter, D.N., Hanspers, K., Miller, R.A., Digles, D., Lopes, E.N., Ehrhart, F., et al. (2021). WikiPathways: Connecting communities. Nucleic Acids Res *49*. 10.1093/nar/gkaa1024.

130. Erratum: SynergyFinder 2.0: Visual analytics of multi-drug combination synergies (Nucleic Acids Research (2020) 48:W1 (W488-W493) DOI: 10.1093/nar/gkaa216) (2022). Nucleic Acids Res *50*. 10.1093/nar/gkac552.

131. Bankhead, P., Loughrey, M.B., Fernández, J.A., Dombrowski, Y., McArt, D.G., Dunne, P.D., McQuaid, S., Gray, R.T., Murray, L.J., Coleman, H.G., et al. (2017). QuPath: Open source software for digital pathology image analysis. Sci Rep *7*. 10.1038/s41598-017-17204-5.

132. Schmidt, U., Weigert, M., Broaddus, C., and Myers, G. (2018). Cell detection with star-convex polygons. In Lecture Notes in Computer Science (including subseries Lecture Notes in Artificial Intelligence and Lecture Notes in Bioinformatics) 10.1007/978-3-030-00934-2_30.

133. Shema, E., Jones, D., Shoresh, N., Donohue, L., Ram, O., and Bernstein, B.E. (2016). Single-molecule decoding of combinatorially modified nucleosomes. Science (1979) *352*. 10.1126/science.aad7701.

Figure 1

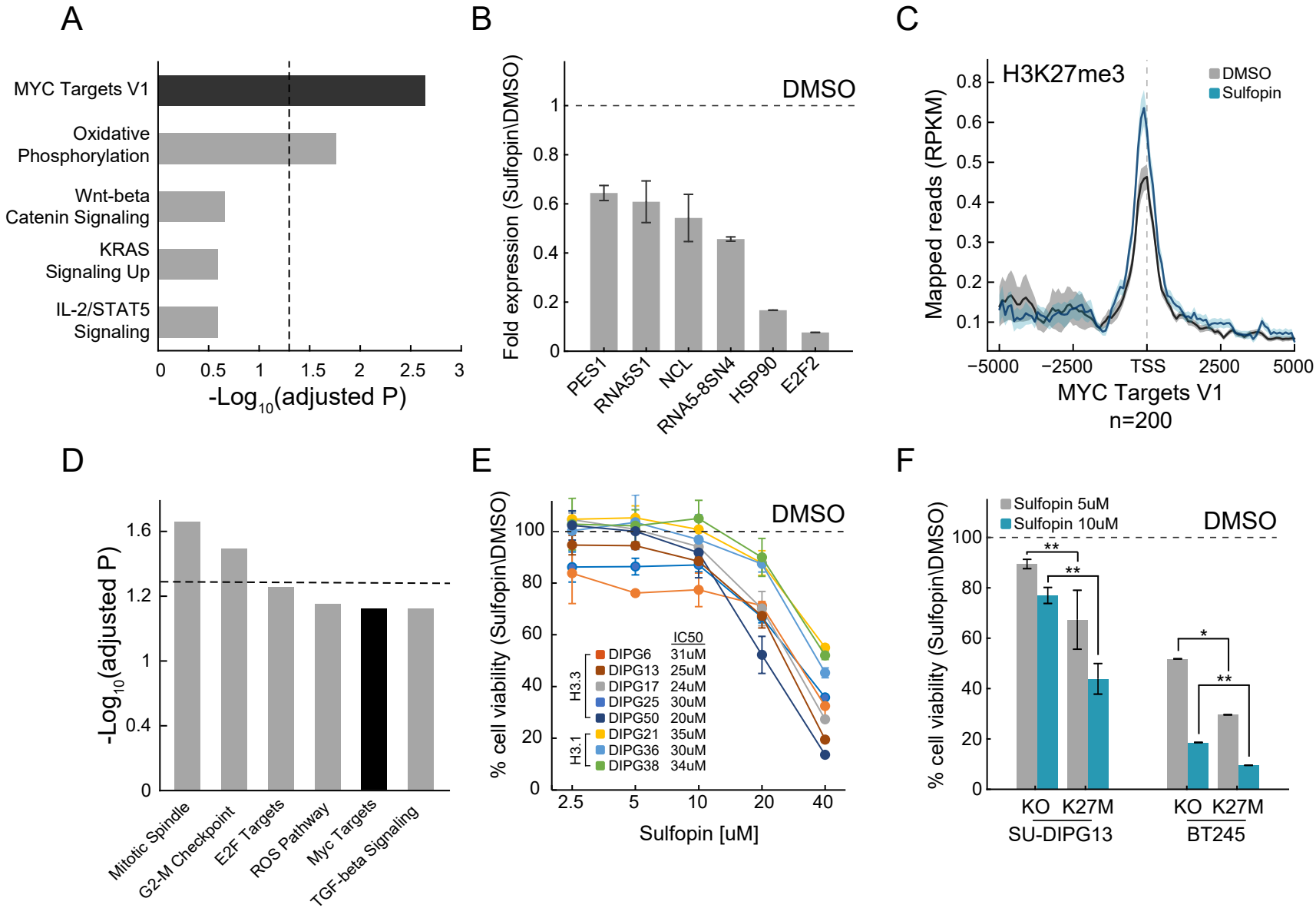
A
MYC Targets V1
Oxidative Phosphorylation
Wnt-beta Catenin Signaling
KRAS Signaling Up
IL-2/STAT5 Signaling
0
0.5
1
1.5
2
2.5
3
-Log10(adjusted P)
B
DMSO
Fold expression (Sulfopin\DMSO)
1
0.8
0.6
0.4
0.2
0
PES1
RNA5S1
NCL
RNA5-8SN4
HSP90
E2F2
C
H3K27me3
DMSO
Sulfopin
Mapped reads (RPKM)
0.8
0.6
0.5
0.4
0.3
0.2
0.1
−5000
−2500
TSS
2500
5000
MYC Targets V1
n=200
D
-Log10(adjusted P)
1.6
1.2
1
0.4
0
Mitotic Spindle
G2-M Checkpoint
E2F Targets
ROS Pathway
Myc Targets
TGF-beta Signaling
E
DMSO
% cell viability (Sulfopin\DMSO)
100
80
60
40
20
0
IC50
H3.3
DIPG6 31uM
DIPG13 25uM
DIPG17 24uM
DIPG25 30uM
DIPG50 20uM
H3.1
DIPG21 35uM
DIPG36 30uM
DIPG38 34uM
2.5
5
10
20
40
Sulfopin [uM]
F
Sulfopin 5uM
Sulfopin 10uM
DMSO
% cell viability (Sulfopin\DMSO)
100
80
60
40
20
0
**
**
*
**
KO
K27M
KO
K27M
SU-DIPG13
BT245

Figure 2

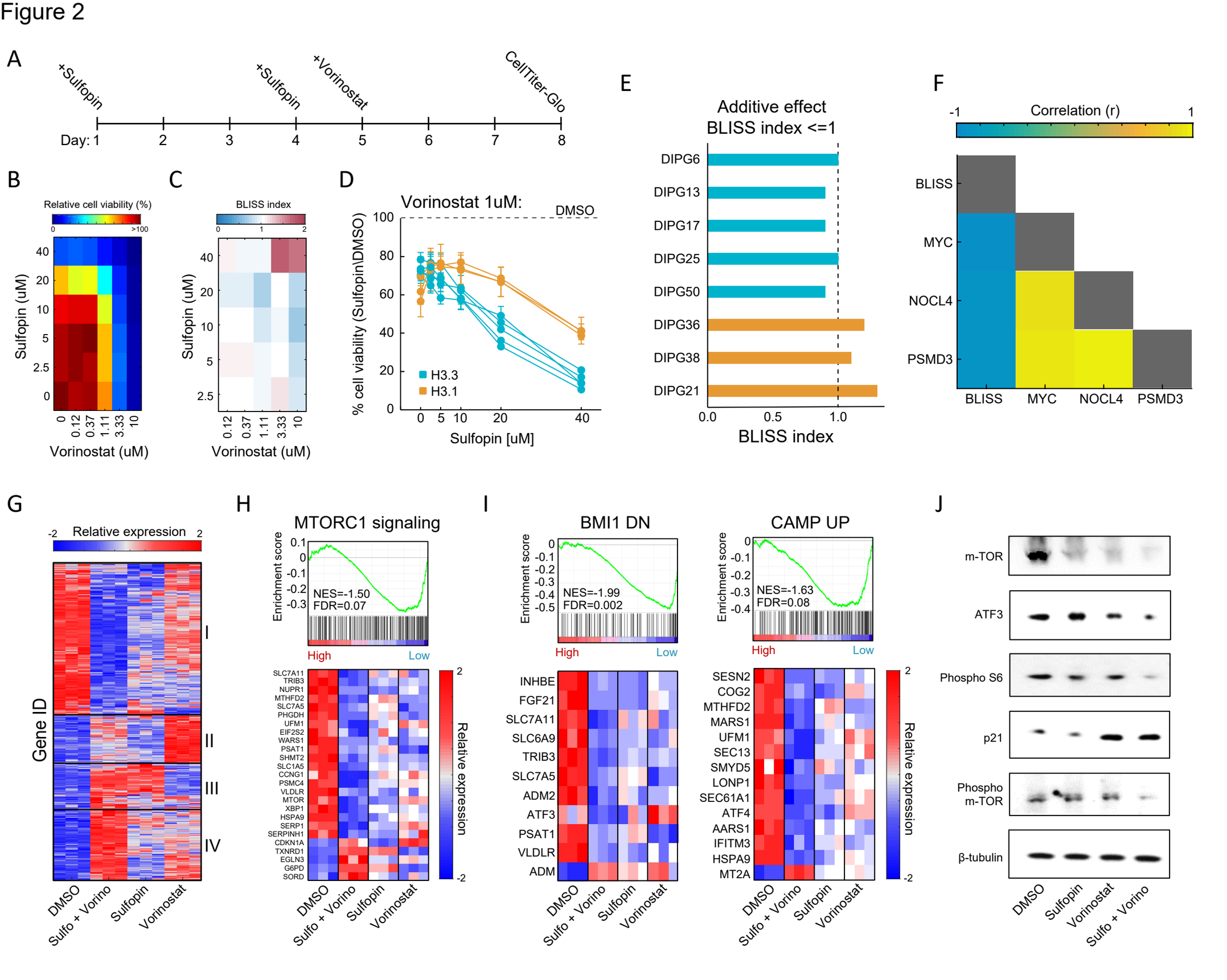
A
+Sulfopin
+Sulfopin
+Vorinostat
CellTiter-Glo
Day: 1 2 3 4 5 6 7 8
B
Relative cell viability (%)
0 >100
Sulfopin (uM)
40 20 10 5 2.5 0
0 0.12 0.37 1.11 3.33 10
Vorinostat (uM)
C
BLISS index
0 1 2
Sulfopin (uM)
40 20 10 5 2.5
0.12 0.37 1.11 3.33 10
Vorinostat (uM)
D
Vorinostat 1uM:
DMSO
% cell viability (Sulfopin\DMSO)
100 80 60 40 20 0
H3.3
H3.1
0 5 10 20 40
Sulfopin [uM]
E
Additive effect
BLISS index <=1
DIPG6
DIPG13
DIPG17
DIPG25
DIPG50
DIPG36
DIPG38
DIPG21
0.0 0.5 1.0
BLISS index
F
-1 Correlation (r) 1
BLISS
MYC
NOCL4
PSMD3
BLISS MYC NOCL4 PSMD3
G
-2 Relative expression 2
Gene ID
I
II
III
IV
DMSO
Sulfo + Vorino
Sulfopin
Vorinostat
H
MTORC1 signaling
Enrichment score
0.1 0 -0.1 -0.2 -0.3
NES=-1.50
FDR=0.07
High
Low
SLC7A11
TRIB3
NUPR1
MTHFD2
SLC7A5
PHGDH
UFM1
EIF2S2
WARS1
PSAT1
SHMT2
SLC1A5
CCNG1
PSMC4
VLDLR
MTOR
XBP1
HSPA9
SERP1
SERPINH1
CDKN1A
TXNRD1
EGLN3
G6PD
SORD
2
Relative expression
-2
DMSO
Sulfo + Vorino
Sulfopin
Vorinostat
I
BMI1 DN
Enrichment score
0 -0.1 -0.2 -0.3 -0.4 -0.5
NES=-1.99
FDR=0.002
High
Low
INHBE
FGF21
SLC7A11
SLC6A9
TRIB3
SLC7A5
ADM2
ATF3
PSAT1
VLDLR
ADM
CAMP UP
Enrichment score
0 -0.1 -0.2 -0.3 -0.4
NES=-1.63
FDR=0.08
High
Low
SESN2
COG2
MTHFD2
MARS1
UFM1
SEC13
SMYD5
LONP1
SEC61A1
ATF4
AARS1
IFITM3
HSPA9
MT2A
2
Relative expression
-2
DMSO
Sulfo + Vorino
Sulfopin
Vorinostat
J
m-TOR
ATF3
Phospho S6
p21
Phospho m-TOR
β-tubulin
DMSO
Sulfopin
Vorinostat
Sulfo + Vorino

Figure 3

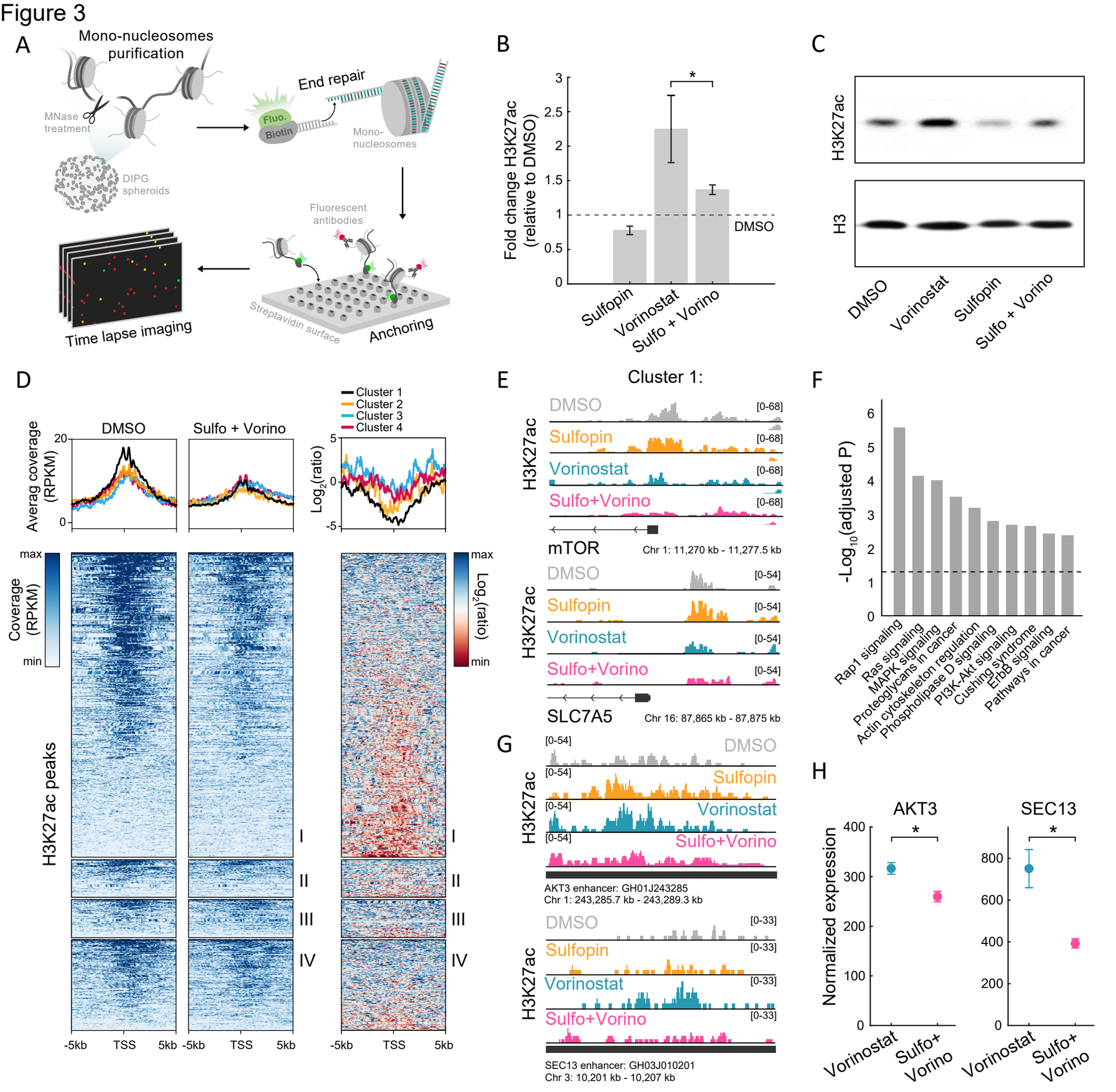
A
Mono-nucleosomes purification
MNase treatment
DIPG spheroids
End repair
Fluo.
Biotin
Mono-nucleosomes
Fluorescent antibodies
Streptavidin surface
Anchoring
Time lapse imaging
B
Fold change H3K27ac (relative to DMSO)
DMSO
Sulfopin
Vorinostat
Sulfo + Vorino
C
H3K27ac
H3
DMSO
Vorinostat
Sulfopin
Sulfo + Vorino
D
Cluster 1
Cluster 2
Cluster 3
Cluster 4
DMSO
Sulfo + Vorino
Averag coverage (RPKM)
Log2(ratio)
Coverage (RPKM)
max
min
H3K27ac peaks
I
II
III
IV
-5kb
TSS
5kb
E
Cluster 1:
H3K27ac
DMSO
Sulfopin
Vorinostat
Sulfo+Vorino
mTOR
Chr 1: 11,270 kb - 11,277.5 kb
SLC7A5
Chr 16: 87,865 kb - 87,875 kb
F
-Log10(adjusted P)
Rap1 signaling
Ras signaling
MAPK signaling
Proteoglycans in cancer
Actin cytoskeleton regulation
Phospholipase D signaling
PI3K-Akt signaling
Cushing syndrome
ErbB signaling
Pathways in cancer
G
AKT3 enhancer: GH01J243285
Chr 1: 243,285.7 kb - 243,289.3 kb
SEC13 enhancer: GH03J010201
Chr 3: 10,201 kb - 10,207 kb
H
AKT3
SEC13
Normalized expression
Vorinostat
Sulfo+ Vorino

Figure 4

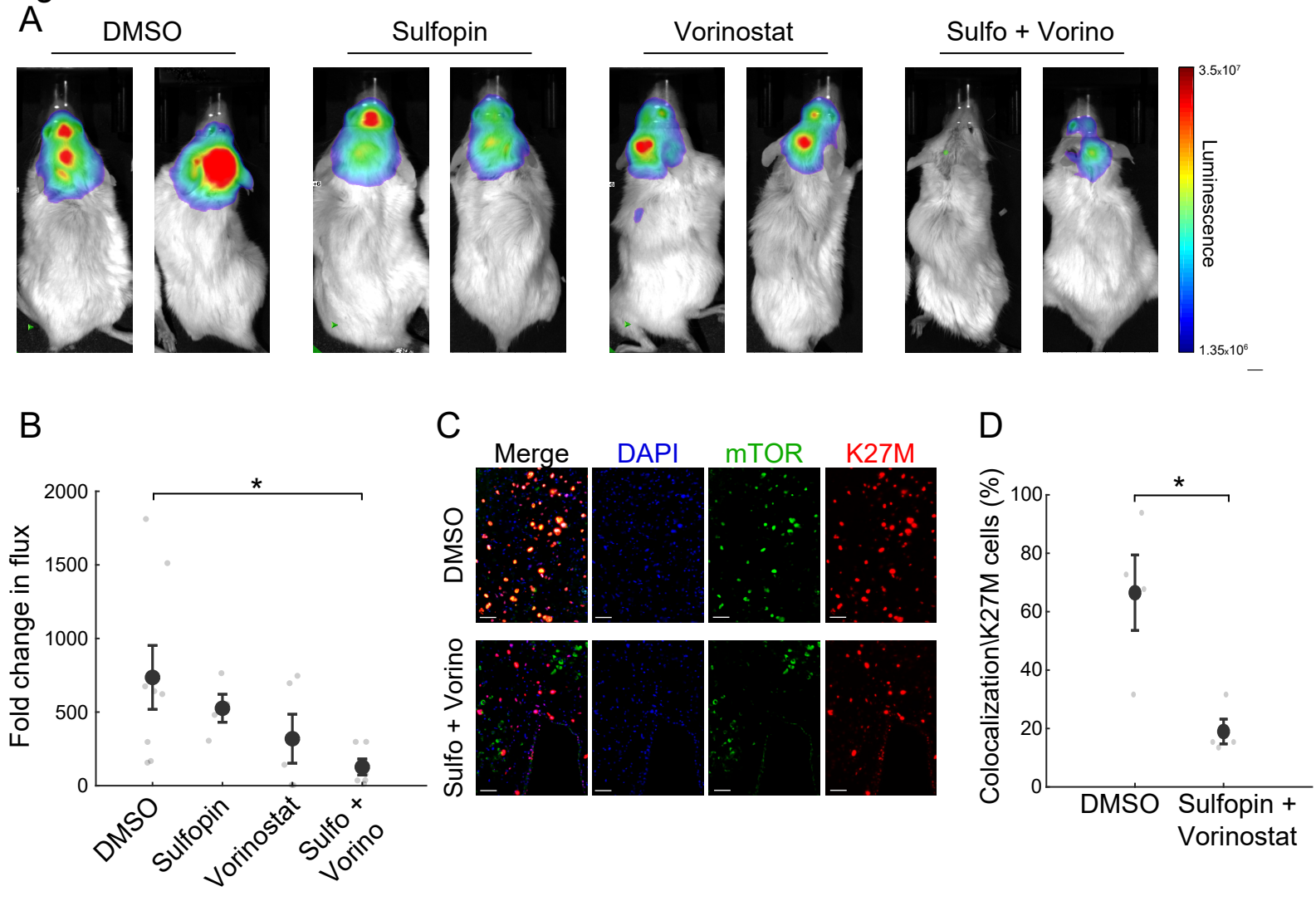
A
DMSO
Sulfopin
Vorinostat
Sulfo + Vorino
3.5x10^7
Luminescence
1.35x10^6
B
Fold change in flux
2000
1500
1000
500
0
*
DMSO
Sulfopin
Vorinostat
Sulfo + Vorino
C
Merge
DAPI
mTOR
K27M
DMSO
Sulfo + Vorino
D
Colocalization\K27M cells (%)
100
80
60
40
20
0
*
DMSO
Sulfopin + Vorinostat